# Flow velocity analysis of lee side "Wide Green Dike" using Swash

M.E. Rekveld BSc

4864727 30/06/2022



**TU**Delft

# Flow velocity analysis of lee side "Wide Green Dike" using Swash

by

M.E. Rekveld BSc

to obtain the degree of Master of Science at the Delft University of Technology, to be defended publicly on Monday 30 June, 2022 at 10:30 AM.

Student number: 4864727

Project duration: September 1, 2021 – June 30, 2022 Thesis committee: Dr. ir. B. Hofland, TU Delft, supervisor

Dr. A. Antonini, TU Delft

ir. H.L. Maris, Sweco Nederland B.V.

An electronic version of this thesis is available at http://repository.tudelft.nl/.



## **Abstract**

The water authority "Hunze en Aa's" initiated a demonstration project adjacent to the Dollard where non traditional dike reinforcement strategies could be developed. For this project Sweco designed a sea dike with an outer slope more gentle than traditional. This dike is called the "Wide Green Dike" (WGD) and has an outer slope of 1:7. This dike is designed for 10 l/s/m overtopping with hydraulic boundary conditions provided by HYDRA-NL. This report examines whether 10 l/s/m of overtopping leads to failure of the WGD. In this context failure means erosion of the inner dike slope. Whether failure occurs is based upon the cumulative overload method (Steendam et al., 2015).

The WGD is rebuilt in a computational model called SWASH <sup>1</sup>, which is a general-purpose numerical tool for simulating non-hydrostatic, free-surface, rotational flows and transport phenomena in one, two or three dimensions. The flow velocities on the rebuilt dike for the overtopping design condition are analysed. In this study SWASH is used to analyse 2D wave interactions from nearshore along a shallow foreshore towards and over a sea dike. According to literature SWASH can be used for assessing overtopping flows (Gruwez et al., 2020), however it was not used for such gentle dike slopes up to now. To verify whether SWASH can assess overtopping flows on a gentle outer dike slope, SWASH is compared with physical model tests by Schüttrumpf et al. (2001) (test nr. 3105009). The validation concluded that SWASH predicts reality reasonably well. Considering overtopping events, SWASH showed good agreement with the peak flow velocities but overestimated the trailing flow velocities. The trailing flow velocities could potentially influence the flow further downstream. Given the fact that the inaccuracy is an overestimation instead of an underestimation would indicate that the model outcome is more conservative. Therefore, the overestimation of the trailing flow velocities is considered unfortunate but not a blocking issue for the outcome of this research.

The model was further verified by a sensitivity analysis for certain model settings to optimize the model performance. To elaborate, the breaking waves of this physical model test by Schüttrumpf et al. (2001) are of the plunging type. It turns out that the waves of the WGD model are of the plunging type as well. SWASH is a depth integrated model and consequently any configuration with more than two solids in the vertical direction cannot be applied (Suzuki et al., 2017). Therefore separation due to splash air-entertainment (e.g., plunging waves) are not represented in the model. However, Suzuki et al. (2017) compared the predicted energy dissipation due to plunging breakers by SWASH with physical model tests and concluded that SWASH represents the energy dissipation reasonable well due to the shock capturing feature and hydrostatic front approximation. The hydrostatic front approximation is tuned with the "break" statement. The "break" statement is one of the model settings included in the sensitivity analysis. The other parameters included in sensitivity analysis are the depmin parameter, which checks for flooding and drying and the numbers of layers in the vertical. The results from the validation/sensitivity analysis in this paper show that although the breaking waves are plunging and SWASH being a depth integrated model that due to the hydrostatic front approximation SWASH represents reality reasonably well. It provides confidence, besides the confirmation from literature (Suzuki et al., 2017), that SWASH simulates breaking waves in the WGD model with reasonable accuracy.

Next, the WGD is considered. The wave boundary condition is provided by HYDRA-NL. HYDRA-NL extrapolates wave data from the Nordsea to the Dollard using SWAN <sup>2</sup>. However, a closer look to the provided wave climate shows that the predicted wave climate is most likely physically impossible. To specify, the Kamphuis (1997) and Miche (Schiereck and Verhagen, 2012) wave steepness criterion is violated, the combination of wave height and wave period cannot occur. Consequently, modelling the exact conditions the dike was designed for is not possible.

This resulted in the formulation of new hydraulic boundary conditions. No wave records exist for the Dollard that could give an indication of the wave climate. Several options for the wave boundary con-

<sup>&</sup>lt;sup>1</sup>Simulating WAves till SHore

<sup>&</sup>lt;sup>2</sup>Simulating WAves Nearshore

ditions are discussed. For example to assume that the wave height was predicted correctly but the wave period was not. The sinuous shape of the estuary makes it however arguable whether waves that are generated in the Nordsea are able to reach the Dollard and eventually the dike. It is therefore concluded that the waves are most likely generated inside the Dollard. The wave boundary condition is therefore calculated using an empirical fetch based wave generation formula.

The empirical fetch based wave generation formula results in waves arriving at the toe with  $H_s=1.3$  m and  $T_{peak}=4.0$  s. This results in an Iribarren breaker parameter of  $\xi=0.63$ , which is in the plunging breaker regime (0.5 <  $\xi$  < 3, Schiereck and Verhagen, 2012). As mentioned above the breakers being of the plunging type will not be a problem for analysing the flow over the dike.

The simulation using the locally generated waves results in no overtopping. The overtopping criterion is normative for the crest height and no overtopping indicates that it is likely that the design of the dike can be optimized. But before any decisive conclusion can be made more research into the wave climate in the Dollard is needed.

As the scenario using the locally generated waves resulted in no overtopping, a new scenario is created. This scenario has other wave boundary conditions, such that there is overtopping. This simulation results in 57 l/s/m overtopping but without any initiation of damage on the lee side according to the cumulative overload method. This result would indicate that exceeding an average overtopping of 10 l/s/m might not necessary lead to failure for a dike with a more gentle, compared to standard, outer slope.

This scenario also shows that the flow velocity on the crest is not a continuous flow velocity decrease towards the end of the crest but a significant initial flow velocity decrease after which the flow velocity only slightly decreases as the overtopping wave travels towards the end of the crest. Consequently the equations that predict the flow velocity on the crest highly underestimate the flow velocity.

The same simulation shows that the current relation for the flow on the lee side is likely not sufficient to describe the full flow pattern. According to literature the flow velocity on the lee side of a dike increases and stabilizes. However, SWASH simulation results show after the initial increase also a decrease in flow velocity. The current relations for the flow velocity on the lee side only include the first initial increase but do not include the observed decrease in flow velocity. The kinematic shock theory equation, shows good agreement with the decrease in velocity. The results show that the tipping point (change from flow velocity increase to decrease) is located at 97% of the predicted final flow velocity (Van Gent equation). It seems that a combination of the Van Gent equation and kinematic shock equation can represent the flow velocity along the lee side of a dike.

# Contents

Lis	of symbols	vii
1	ntroduction         I.1 Problem definition and research objective          I.2 Approach          I.3 Outline	4
2	Dvertopping 2.1 Tolerable overtopping 2.1.1 Grass strength 2.2 Flow description 2.2.1 Overtopping. 2.2.2 Run-up 2.2.3 Seaward slope 2.2.4 Crest 2.2.5 Landward slope dike 2.3 Erosion due to overtopping 2.3.1 Cumulative overload method 2.3.2 Erosional equivalence	8 9 9 10 11 15
3	Offshore boundary conditions 3.1 Initial boundary conditions	
4	SWASH  4.1 Verification SWASH  4.1.1 Set-up Schüttrumpf SWASH simulation  4.1.2 Breaker parameter  4.1.3 Depmin parameter  4.1.4 Multiple layers  4.1.5 Irregular waves  4.1.6 Summary Schüttrumpf test  4.2 "Wide Green Dike" SWASH model  4.2.1 Bathymetry and dike geometry  4.2.2 Model settings  4.2.3 Model limitations considering wave breaking  4.2.4 Overtopping parameter q.  4.2.5 Post-processing	24 29 29 29 30 31 31 32
5	Results wind based wave conditions Results of an extended analysis of flow velocity behaviour crest Results of an extended analysis of flow velocity behaviour lee side S.3.1 Kinematic Shock theory S.4 Effect different outer slope	34 35 38
-		
7		<b>53</b> 54

vi	Contents

Α	Han	d calculation flow crest and lee side WGD	57
	A.1	Flow seaward	58
	A.2	Flow crest	58
	A.3	Flow lee side	59

# List of symbols

The following is a list of the most important symbols in this thesis. The symbols are arranged by order of appearance.

$H_{m0}$	Significant wave height	[m]
q	Overtopping	[m/s/m] or [l/s/m]
g	Gravititational accelaration constant = 9.81	$[m/s^2]$
α	Dike outer slope	[-]
$R_c$	Freeboard	[m]
$\gamma_f$	Roughness influence factor	[-]
$\gamma_{m{\phi}}$	Wave obliqueness influence factor	[-]
$\gamma_v$	Wall or promenade influence factor	[-]
$\xi_{m-1,0}$	Iribarren parameter	[-]
φ	Wave angle of incidence	[-]
$r_{\!\scriptscriptstyle B}$	Influence of width of the berm	[-]
$r_{db}$	Stands for the vertical difference $d_b$ between the still water level (SWL) and the middle of the berm	[-]
$d_b$	Height between berm and still water level	[m]
$L_{berm}$	Characteristic berm length	[m]
$v_{A,50\%}$	Wave run-up velocity on the seaward slope exceeded by 50% of the incoming waves	[-]
$k^*$	Dimensionless coefficient	[-]
$R_{u,2\%}$	Wave run-up height exceeded by 2%	[m]
$z_A$	Vertical coordinate with respect to sea water level (SWL)	[m]
$u_{A,2\%}$	Wave run-up velocity exceeded by 2%	[m/s]
$C_{A,u}^*$	Empirical coefficient	[-]
$h_{A,2\%}$	Layer thickness on the seaward slope exceeded by 2% of the incoming waves	[m]
$c_{A,h}^*$	Empirical coefficient	[-]
$u_{c,2\%}$	Wave overtopping velocity on the crest exceeded by 2% of the incoming waves	[m/s]
$h_{c,2\%}$	Layer thickness on the crest exceeded by 2% of the incoming waves	[m]
$C_{C,u}^*$	Empirical coefficient	[-]
f	Position on the dike crest with respect to the beginning of the dike crest	[m]
f	Friction coefficient	[-]
$B_c$	Crest width	[m]
${f C}^*_{C,u} \ {f Q}$	Empirical coefficient	[-]
	Discharge	$[m^3/s]$
$U_{c0}$	Velocity at the start of the dike crest	[m/s]
$v_0$	Overtopping velocity at beginning of the landward slope	[m/s]
$h_0$	Layer thickness at beginning of the landward slope	[m]
β	Slope angle inner slope	[-]
$S_B$	Position on the inner slope with respect to the beginning of the inner slope	[m]
$u_c$	Critical flow velocity	[m/s]
L	Wave length	[m]
d	Water depth	[m]
$H_b$	Individual wave height	[m]
$H_{\mathcal{S}}$	Significant wave height	[m]
$L_{ ilde{m{p}}}$	Wave length of breaking waves calculated using the peak period	[m]
ď	Dimensionless depth	[-]
$U_{10}$	Wind velocity at 10 m above water surface	[m/s]
F	Dimensionless fetch	[-]
F	Fetch	[m]
$H^{m_0}$	Dimensionless wave height	[-]
$T^{peak}$	Dimensionless wave period	[-]
$c_f$	Friction constant	[-]
и	Flow velocity	[m/s]

1

## Introduction

Historically, the protection of the Dutch hinterland against flooding is a recurring theme. It is not only a major topic of today but it has shaped the Netherlands throughout history. The presence of dikes, sluices, weirs and other flood defence structures are leading in the Dutch landscape. Years of experience and research made the knowledge of building flood defence structures develop immensely. Eventually throughout the years the flood protection strategy has changed. In the beginning it used to be working against nature. Nowadays the focus has shifted to a working with nature approach, which is e.g. shown in the project "room for the river" (Rijkswaterstaat, 2021b).

This report focuses on one particular flood defence structure, namely dikes, which protect the hinterland from flooding. Dikes have been built for many years, the oldest dike is even estimated to be from the  $11^{th}$  century (Rijkswaterstaat, 2021a). The total dike length in the Netherlands sums up to 17500 km and can be subdivided between 3500 km of primary dikes and 14600 km of secondary dikes (UVW, 2021). Primary flood defences protect against open water, the IJssel- en Markermeer and large rivers and the secondary flood defences protect against small rivers, lakes and canals (Rijkswaterstaat, 2021c). Dikes can be subdivided into three types, sea dikes, river dikes and lake dikes (Rijkswaterstaat, 2021a). Each type has its own characteristics. Dikes are designed site specific, this means that each dike is designed purpose specific. River dikes experience long-lasting high-water levels and thus a large head difference over the dike, the design focus lies on protection against failure mechanisms that affect the inner dike slope such as piping. Sea dikes are less likely to experience a large head difference but are prone to wave attack and need therefore special attention at the outer slope, this often includes a reinforced outer slope (Kremer et al., 2001).

Although dikes are designed location specific they do have standard slopes. The characteristic slopes are presented in table 1.1. Figure 1.1 depicts a standard sea dike, with an outer slope of 1:4 and an inner slope of 1:3.

Table 1.1: Typical slopes of different dike types(Van den Bos, 2006).

Type of dike	Characteristic slope of dikes in the Netherlands (horizontal : vertical)	
	Outer slope Inner slope	
River	1:2 - 1:3	1:2 - 1:3
Lake	1:3	1:2 - 1:2.5
Sea	1:4	1:2.5 - 1:3

2 1. Introduction

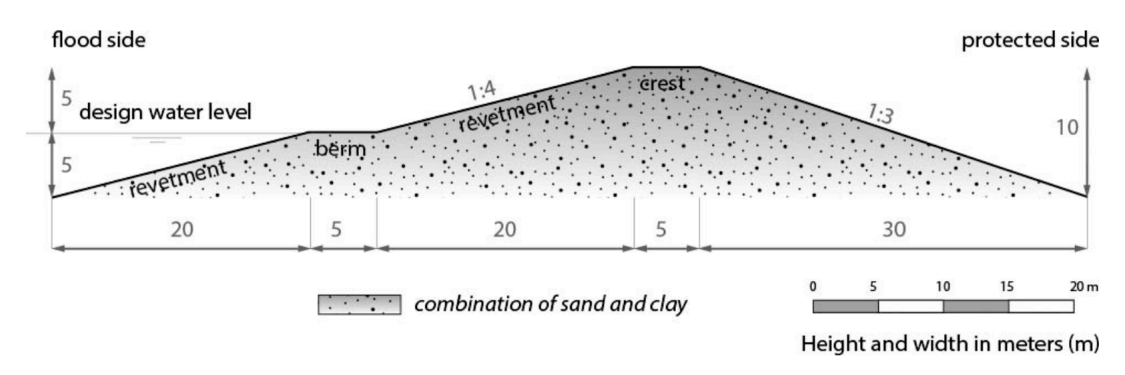


Figure 1.1: Standard dutch sea dike (Jonkman et al., 2013).

Dikes are designed to withstand several failure mechanisms, such as e.g. piping, sliding and overtopping. Severe overtopping causes erosion of the inner slope with dike failure as potential consequence. This thesis focuses on erosion of the inner slope due to overtopping on a special type of dike design with a gentle outer slope.

The water authority "Hunze en Aa's" is located in North-East Drenthe and East Groningen and is responsible for 28 km of primary flood defence structures and 795 km of secondary flood defences (Waterschap-Hunze-en-Aa's, 2021). One of these structures is the sea dike adjacent to the Dollard. All primary flood defence structures are judged periodically and found sufficient or insufficient conform the Dutch national legal norms. The sea dike adjacent to the Dollard is found insufficiently strong. It follows that this dike needs to be reinforced such that it meets the Dutch standard norm. Traditional reinforcement would include an asphalt or rubble mount revetment. However, the dike is situated in one of the Natura 2000 areas and the water authority "Hunze en Aa's" wanted to preserve the area's ecological value (Waterschap-Hunze-en-Aa's, 2021). Consequently, the new dike had to be "green" and smart". This initiated a 1 km demonstration project where non-traditional dike reinforcement strategies" could be developed. This demonstration dike is designed by Sweco and called the "Brede Groene Dijk" (or "Wide Green Dike"), hereafter referred to as "WGD". The project is finalized in 2022. The dike has a 1:7 outer slope, which is more gentle than traditional sea dikes. The dike is consequently much wider, which explains the name. The WGD is a dike of 1 km length and covered with grass, hence "green". To reinforce 1 km of dike a total of 1 700 000  $m^3$  of clay is needed (Dijk, 2021). This raises the question of where to find such large amounts of clay. This is where the project requirement "smart" comes in (SWECO, 2021a). The required clay is extracted from the Eems-Dollard estuary, by means of clay ripening projects. The Eems-Dollard estuary experiences too high turbidity levels causing disruption of flora and fauna ("HET VERHAAL VAN DE EEMS-DOLLARD", 2021). Any clay extraction would help reducing turbidity levels and thus help create a more sustainable estuary. This approach fits nicely in the building with nature design philosophy mentioned in the first paragraph.



Figure 1.2: Enlarged overview of Waddensea area, the Dollard and Kerkhovenpolder-Duitsland (SWECO, 2021b)



Figure 1.3: Aerial photo of the Dollard with project location depicted in red square. (SWECO, 2021b)

The WGD has a lifetime of 50 years and an overall failure probability of 1/3000 per year (SWECO, 2021b). The maximum allowable overtopping criterion is set to 10 l/s/m and the overtopping failure mechanism has a maximum exceeding probability of 1/37500 per year. During the design phase, the overtopping failure criteria appeared normative for the crest height. The geometry of the WGD is shown in figure 1.4. The outer slope consist of a 1:7 slope and a berm of 3 meter width. The berm has a slope of 1:20 and is situated below design water level at 3.55 m +NAP to 3.7 m +NAP. The berm mainly functions as maintenance road and safe haven for cows. The crest level is situated 9 m +NAP and has a width of 11 m. A crest width of 11 m can be considered rather large in comparison with other dikes. The large crest width is because the WGD project is a reinforcement project and consequently build on top of an existing dike. The existing dike has a 1:5 outer slope. In the design phase is decided to keep the old dike intact and to put the clay of the new dike simply on top of the old dike. This means that there is no excavation of the old dike. This results in the crest width of 11 m. If the old dike would be excavated before realisation of the new dike the crest width could be shortened to 4 m instead of 11 m and still meet all design requirements. The lee side of the dike has a 1:3 inner slope.

4 1. Introduction

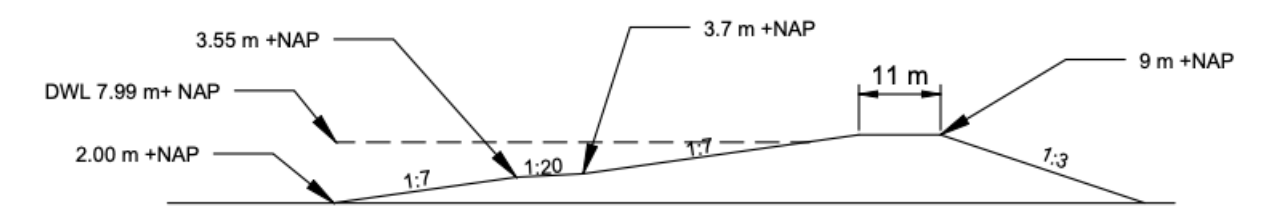


Figure 1.4: Schematic to scale representation of the WGD, left sea side and right the lee side.

#### 1.1. Problem definition and research objective

Overtopping is defined as the average amount of run up in I/s/m that exceeds the sea ward side of the dike and reaches the crest. The current maximum allowable overtopping criterion is derived by means of large-scale physical model tests and justified by visual observation and expert judgement (Smith et al., 1994). Exceeding of these maximum allowable overtopping values would cause failure of the dike. In this context failure means erosion of the inner slope of a dike. The dike in this physical model test had a 1:4 outer slope, it follows that the maximum allowable overtopping criterion is valid for a 1:4 outer slope. The present day used maximum allowable overtopping criterion for dikes is (Van der Meer, 2002):

• 10 l/s/m for a clay covering and a grass cover according to the requirements for the outer slope or for an armoured inner slope.

This thesis examines whether the 10 l/s/m overtopping criterion is also valid for the WGD, which has an 1:7 outer slope. Other related sub objectives are:

- Analyse whether SWASH (computational model) can be used to assess overtopping flows on dikes with a gentle outer slope;
- · Analyse flow velocity behaviour on the lee side;
- Analyse influence of the wide crest on the flow velocities.

#### 1.2. Approach

To analyse the overtopping and flow over the WGD, the computational model SWASH is used. SWASH is a general-purpose numerical tool for simulating non-hydrostatic, free-surface, rotational flows and transport phenomena in one, two or three dimensions. The governing equations are the nonlinear shallow water equation including non-hydrostatic pressure and some transport equations (TU-Delft, 2021).

In this study SWASH is used to analyse 2D wave interactions from nearshore along a shallow foreshore to and over a sea dike. According to literature SWASH can be used for assessing overtopping flows (Gruwez et al., 2020), however it was not used for such gentle dike slopes up to now. To verify whether SWASH can assess overtopping flows on a gentle outer dike slope, SWASH is compared with physical model tests by Schüttrumpf et al. (2001) (test nr. 3105009). This verification also includes a sensitivity analysis for certain model settings to optimize the model performance.

The behaviour of the flow over the dike is analysed by means of the  $u_{2\%}$  velocity and flow equations from literature (see section 2). SWASH calculates the flow velocity (u) and flow depth over the dike. A depth criterion of 0.01 m is applied as threshold. This means, considering the data post-processing, if the flow depth is below the threshold the flow velocity is not taken into account. The velocity data is converted to a  $u_{2\%}$  velocity using a statistical peak over threshold method combined with linear regression. The  $u_{2\%}$  velocity is compared with flow equations from literature that describe the flow on the crest and lee side of a dike.

To assess whether dike failure and erosion occur the cumulative hydraulic load is used (see chapter 2). The cumulative hydraulic load is an erosional index for the grass cover of the inner slope, it is based upon the shear stress with threshold theory (Hoffmans et al., 2008).

1.3. Outline 5

#### 1.3. Outline

This main topic in this thesis is overtopping. It it therefore important to have a clear understanding of the phenomenon. To accommodate insight in the matter the first chapter provides a literature study about overtopping. It presents a clear definition of overtopping, mentions tolerable overtopping values, couples flow velocities to erosion and describes the flow over the dike with help of analytical equations. Having described overtopping, the next chapter discusses the offshore boundary condition for the WGD computational model. The offshore boundary conditions consist of a wave climate. Before any computational modelling can be done the boundaries should be defined.

After the offshore boundary is clear the remaining computational model settings can be defined. This is discussed in the next chapter, which is called *SWASH*. This chapter not only contains the WGD model settings but also a SWASH verification. As discussed, according to literature SWASH can be used for assessing overtopping flows, however it was not used for such gentle outer dike slopes. This chapter checks whether SWASH can be used for overtopping flows on a dike with a gentle outer slope. This implies that SWASH is compared with physical model tests by Schüttrumpf et al. (2001) (test nr. 3105009). This verification also includes a sensitivity analysis for certain model settings to optimize the model performance.

After the model validation is complete and all model settings are defined the model is ready to run. It follows that the next chapter contains the results. After the results follow the discussion, conclusion and finally the recommendations.

# Overtopping

Imagine the following situation, a typical Dutch gentle foreshore with a standard sea dike. Waves travel from the ocean towards the shore, once they reach shallower area they start to break. The breaking waves reach the sea dike and cause run up. In most cases the run up does not reach the crest of the dike and runs down the same outer slope. However, in some cases, the wave height in combination with the water level cause the run up to reach the crest where it runs down the inner slope (see figure 2.1). This is called *green water* overtopping (*Eurotop*, 2018), which is overtopping in classical sense. Another overtopping form is spray or white water overtopping (Eurotop, 2018). Spray occurs when waves break on the outer slope, the generated spray is then carried over the dike by means of its own momentum or by wind. Waves approach the shore randomly in height and time and as overtopping is caused by waves. It follows that also overtopping is random in time, space and volume. Overtopping is defined as the average discharge per linear meter of width (Eurotop, 2018) and thus results in m3/s per m or l/s per m. It is noteworthy that this is a mean value, a lot of small waves can cause the same mean overtopping as fewer large waves. However, larger waves cause more severe overtopping and thus erosion than smaller waves (Eurotop, 2018). The overtopping wave volume describes the individual overtopping volume per wave and is noted as m3 per m. This paper focuses on green water overtopping phenomena.

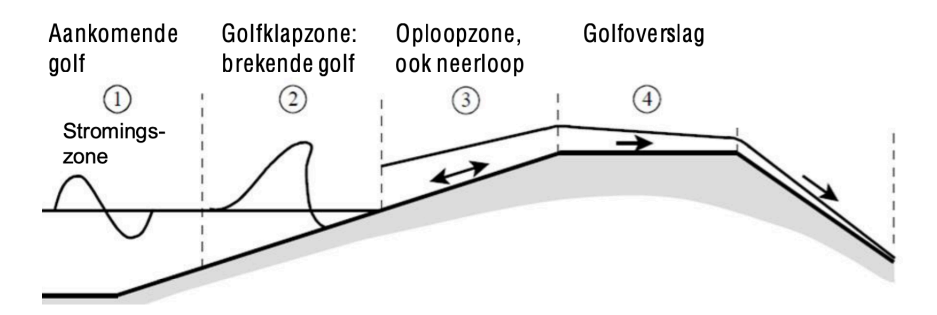


Figure 2.1: Overtopping definition, 1 = wave entering shore, 2 = breaker zone, 3 = run-down and run-up zone, 4 = overtopping zone (Van der Meer et al., 2015)

#### 2.1. Tolerable overtopping

The amount of overtopping that is considered tolerable is variable. It is site specific because it depends on the following (*Eurotop*, 2018):

- · the use of the structure itself, including access to defence for public and/or staff;
- · use of the land (or water) behind;

8 2. Overtopping

- extent and magnitude of drainage ditches;
- · damage versus inundation curves;
- · return periods.

Although it is not possible to give precise overtopping limits the Eurotop manual provides some guidance on maximum overtopping values. Table 2.1 present general maximum allowable overtopping values for breakwaters and dikes (*Eurotop*, 2018). It is noteworthy that it shows high variability depending on the quality of the grass slope.

The eurotop manual also states the following about overtopping experiments with the overtopping simulator:

"A good closed grass cover without open holes is very resilient to wave overtopping for wave heights  $H_{m0} < 3m$ . Sometimes mean discharges of q 100 l/s per m could not damage the slope, but a badly maintained grass cover with open holes and a lot of moss may fail well below q < 5 l/s per m. Moreover, transitions and obstacles (such as staircases, transitions to paths or roads, trees, etc.) on the slope may well cause failure before the grass slope itself." (Eurotop, 2018, p. 62)

This also indicates that, to get a better understanding of erosion due to overtopping, it is key to get a clear description on grass strength.

Hazard type and reason	Mean discharge q (I/s per m)	Max volume $V_{max}$ (I per m)
Rubble mound breakwaters;	1	2000 - 3000
$H_{m0} > 5$ ; no damage	ľ	2000 - 3000
Rubble mound breakwaters; $H_{m0} > 5$ ;	5 - 10	10 000 - 20 000
rear side designed for wave overtopping	3 - 10	10 000 - 20 000
Grass covered crest and landward slope;		
maintained and closed grass cover;	5	2000 - 3000
$H_{m0} = 1 - 3m$		
Grass covered crest and landward slope;		
not maintained grass cover, open spots, moss, bare patches;	0.1	500
$H_{m0} < 1m$		
Grass covered crest and landward slope;	5 - 10	500
$H_{m0} < 1m$	3 - 10	300
Grass covered crest and landward slope;	No limit	No limit
$H_{m0} < 0.3m$	INO IIIIIL	INO IIIIII

Table 2.1: Limits for wave overtopping for structural design of breakwaters, seawalls, dikes and dams(Eurotop, 2018)

#### 2.1.1. Grass strength

To quantify grass strength a failure definition needs to be specified. Failure occurs when one of the following occurs (Van der Meer et al., 2015):

- The depth of erosion is larger than the top layer thickness of 0.2 meter;
- A hole size, that is deeper than the top layer thickness of 0.2 meter, of maximum 0.15 square meter is getting larger due to a load.

There are in total 7 methods to determine the strength of grass sods (Bijlard, 2015). These methods however do not determine the exact grass strength of the grass but use grass characteristics that can be related to strength. Furthermore, these methods neglect weak spots which are most likely prone to erosion. This report focuses on flow behaviour and will therefore not discuss any grass strength determination methods.

#### 2.2. Flow description

As mentioned this paper focuses on the inner slope of a dike. Any flow related formulas for the inner slope do not stand on their own but require flow properties from the dike crest and outer slope. It is

2.2. Flow description 9

therefore necessary to investigate the flow pattern over the entire dike and not just the inner slope. The equations are used to calculated the flow over the WGD dike (see appendix A). The following sections provide the run-up, the flow at the seaward slope, flow over the crest and finally flow over the inner slope. Noteworthy, the current knowledge of flow over a dike an thus the presented formulae in the following section for flow velocity and flow depth do not give precise and consistent answers (Van Der Meer et al., 2010).

#### 2.2.1. Overtopping

There are many methods and formulas, both analytical as well as empirical, to describe and predict overtopping (Andersen and Burcharth, 2004). Not all methods will not be discussed in this paper, for any overtopping calculations there will be made use of the following formula (2.1, *Eurotop*, 2018):

$$\frac{q}{\sqrt{g \cdot H_{m0}^3}} = \frac{0.026}{\sqrt{\tan(\alpha)}} \cdot \gamma_b \cdot \xi_{m-1,0} \cdot \exp\left(-(2.5 \frac{R_c}{\xi_{m-1,0} \cdot H_{m0} \cdot \gamma_b \cdot \gamma_f \cdot \gamma_\beta \cdot \gamma_\nu})^{1.3}\right) \tag{2.1}$$

With:

 $H_{m0}$  = significant wave height [m]

 $\alpha$  = slope [-]

 $R_c$  = freeboard [m]

 $\gamma_f$  = roughness influence factor [-]

 $\gamma_{\beta}$  = wave obliqueness influence factor [-]

 $\gamma_b$  = berm influence factor [-]

 $\gamma_v$  = wall or promenade influence factor [-]

 $\xi_{m-1,0}$  = Iribarren parameter [-]

q = overtopping discharge  $[m^3/s \ per \ m]$ 

#### 2.2.2. Run-up

The equations that describe the flow over the dike, require the run-up as input parameter. The run-up is calculated using formula 2.2 as given by *Eurotop* (2018).

$$\frac{R_{u2\%}}{H_{m0}} = 1.75 \cdot \gamma_b \cdot \gamma_f \cdot \gamma_\phi \cdot \xi_{m-1,0} \tag{2.2}$$

With a maximum of:

$$\frac{R_{u2\%}}{H_{m0}} = 1.07 \cdot \gamma_f \cdot \gamma_\phi (4.0 - \frac{1.5}{\sqrt{\gamma_b \cdot \xi_{m-1,0}}})$$
 (2.3)

With:

 $R_{u2\%}$  = wave run-up measured vertically from the still water line exceeded by 2% of the number of incident waves [m]

 $H_{m0}$  = significant wave height [m]

 $\gamma_f$  = roughness influence factor [-]

 $\gamma_{\phi}$  = wave obliqueness influence factor [-]

 $\gamma_b$  = berm influence factor [-]

 $\gamma_v$  = wall or promenade influence factor [-]

 $\xi_{m-1,0}$  = Iribarren parameter [-]

The wave obliqueness influence factor follows from the wave angle of incidence and is given by (equation 2.4):

$$\gamma_{\phi} = 1 - 0.0033|\phi| \tag{2.4}$$

The berm influence factor for a berm below still water line is given by (equation 2.5):

$$\gamma_b = 1 - r_R (1 - rdb) \tag{2.5}$$

10 2. Overtopping

With:

$$r_{db} = 0.5 - 0.5\cos(\pi \frac{d_b}{2 \cdot H_{m0}}) \tag{2.6}$$

And

$$r_B = \frac{B}{L_{Berm}} \tag{2.7}$$

With:

 $d_b$  = height between berm and still water level [m]  $H_{m0}$  = significant wave height [m]  $L_{berm}$  = characteristic berm length [m]

#### 2.2.3. Seaward slope

Schüttrumpf and Van Gent provide an analytical solution (Van Gent and Schüttrumpf, 2004) for the flow velocity (equation 2.9) along the seaward slope of a sea dike. The wave-run up velocities (equation 2.9) can be derived using a simplified energy equation (equation 2.8). Details of the derivation of this formula are described in Schüttrumpf (2001) and confirmed in Schüttrumpf (2001) and Van Gent (2001). See figure 2.2 for definitions.

$$v_{A,50\%} = k^* \cdot \sqrt{2 \cdot g \cdot (R_{u,2\%} - z_A)}$$
 (2.8)

With:

 $v_{\rm A,50\%}$  = wave run-up velocity on the seaward slope exceeded by 50% of the incoming waves

 $R_{u,2\%}$  = wave run-up height exceeded by 2% [m]

 $k^*$  = dimensionless coefficient [-]

 $z_A$  = vertical coordinate with respect to sea water level (SWL) [m]

$$\frac{u_{A,2\%}}{\sqrt{gH_S}} = c_{A,u}^* \cdot \sqrt{\frac{R_{u,2\%} - z_A}{H_S}}$$
 (2.9)

With:

 $u_{A,2\%}$  = wave run-up velocity exceeded by 2% [m/s]  $R_{u,2\%}$  = wave run-up height exceeded by 2% [m]  $z_A$  = position on the seaward slope with respect to SWL [m]  $C_{A,u}^*$  = empirical coefficient [-]

The layer thickness can be determined by assuming a linear decrease of the layer thickness from SWL to  $R_{u,2\%}$  (Van Gent and Schüttrumpf, 2004).

$$\frac{h_{A,2\%}}{H_S} = c_{A,h}^* \cdot (\frac{R_{u,2\%} - z_A}{H_S})$$
 (2.10)

With:

 $h_{A,2\%}$  = layer thickness on the seaward slope exceeded by 2% of the incoming waves [m]

 $c_{A,h}^*$  = empirical coefficient [-]  $R_{u.2\%}$  = wave run-up height [m]

Table 2.2 presents the empirical coefficients derived from Schüttrumpf and Van Gent. The table shows high variability between empirical values. According to Van Gent and Schüttrumpf, 2004 the difference can be explained due to different model set-ups and tests. However, the velocity data retrieved from large scale physical model test by Schüttrumpf appear to be not very reliable. The empirical flow velocity coefficient found by Schüttrumpf is considered too low (Bosman et al., 2009). Bosman et al.

2.2. Flow description 11

Table 2.2: Empirical coefficients for equation 2.9 and 2.10 (Van Gent and Schüttrumpf, 2004)

	Schüttrumpf	Van Gent
run-up velocity $c_{A,u}^*$	1.37	1.3
layer thickness $c_{A,h}^*$	0.33	0.15

(2009) found that the empirical coefficients for the outer slope and crest depend on the outer slope. Bosman et al. (2009) proposes new empirical factor for the outer slope (table 2.3) and crest (table 2.5) and a new formula for the flow velocity (equation 2.14) and flow height (equation 2.13) on the crest.

Table 2.3: Adapted empirical coefficients(Bosman et al., 2009)

	Slope		
	1:7 1:4		
<i>c</i> <sub><i>u</i>,2%</sub>	2.12	1.24	
<i>c</i> <sub>h,2%</sub>	0.45	0.153	

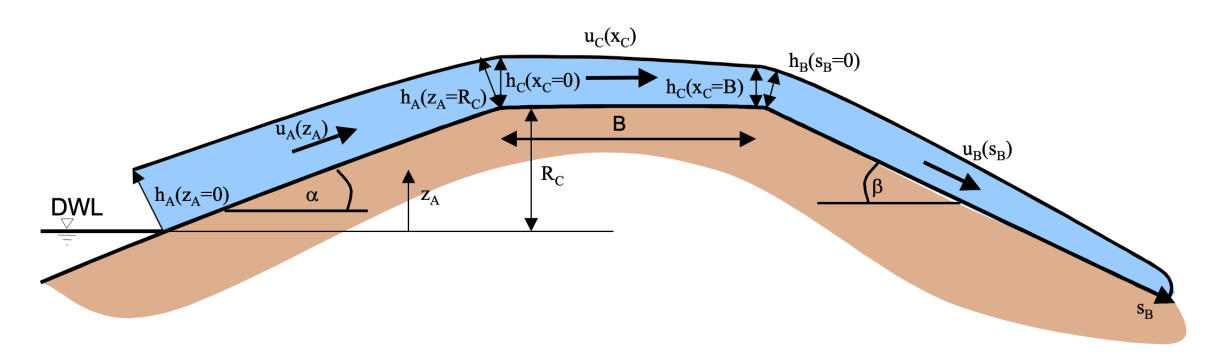


Figure 2.2: Schematic dike cross section defining parameters for equations by Schüttrumpf and Van Gent (Van Gent and Schüttrumpf, 2004)

#### 2.2.4. Crest

The equation for overtopping velocities was determined analytically from the momentum equation (equation 2.11, Van Gent and Schüttrumpf, 2004). A detailed derivation of equation 2.11 is given in Schüttrumpf (2001). See figure 2.2 for definitions.

$$\frac{u_{c,2\%}}{u_{A,2\%}(R_C)} = exp(-c_{c,u}^* \cdot \frac{x_c \cdot f}{h_{c,2\%}})$$
 (2.11)

With:

 $u_{c,2\%}$  = wave overtopping velocity on the crest exceeded by 2% of the incoming waves [m]

 $h_{c,2\%}$  = layer thickness on the crest exceeded by 2% of the incoming waves [m]  $C_{c,u}^*$  = empirical coefficient [-]

 $x_c$  = position on the dike crest with respect to the beginning of the dike crest [m]

f = friction coefficient [-]

 $R_C$  = freeboard [m]

The equation for layer thickness was determined empirically. A detailed derivation of equation 2.12 is given in Schüttrumpf (2001).

$$\frac{h_{c,2\%}}{h_{A,2\%}(R_C)} = exp(-c_{c,h}^* \cdot \frac{x_c}{B})$$
 (2.12)

With:

12 2. Overtopping

 $B_c$  = crest width  $C_{C,u}^*$  = empirical coefficient

Table 2.4: Empirical coefficient for equation 2.11 and 2.12 (Van Gent and Schüttrumpf, 2004)

	Schüttrumpf	Van Gent
- $        -$	0.5	0.5
layer thickness $c_{c,h}^*$	0.89	0.4

Table 2.4 presents the empirical coefficients derived from Schütrrumpf and Van Gent. The difference between coefficients can be explained by different model set-ups and test programs (Van Gent and Schüttrumpf, 2004).

As the flow progresses from outer slope to crest there is a direction change. This transition in direction needs time and space (Bosman et al., 2009). The paper by Bosman et al. (2009) proposes an adaption of equation 2.12, this gives the following formula (equation 2.13):

$$\frac{h_{2\%}(x_c)}{h_{2\%}(x_c = 0)} = c_{trans,h} \cdot \exp(-c_{h,2\%} \cdot \frac{x_c}{\gamma_c \cdot L_0})$$
 (2.13)

Equation 2.11 is adapted into equation 2.14.

$$\frac{u_{2\%}(x_c)}{u_{2\%}(x_c=0)} = \exp(-c_{u,2\%} \cdot \frac{x_c}{\gamma_c \cdot h_{2\%}(x_c)})$$
 (2.14)

The empirical parameters for these equations are given in table 2.5. These parameters are derived for regular waves but the parameters for irregular waves are expected to be similar (Bosman et al., 2009).

Table 2.5: Empirical parameters for equations 2.13 and 2.14 (Bosman et al., 2009)

	Bosman		
$c_{trans,h}$	0.81		
<i>c</i> <sub>h,2%</sub>	15		
<i>c</i> <sub><i>u</i>,2%</sub>	0.042		

Another equation (2.15, see figure 2.4 for parameters) for the flow velocity is published in Van Bergeijk et al. (2019). Derived from the one dimensional shallow water equation. A detailed derivation is presented in Van Bergeijk et al. (2019).

$$U(x) = \frac{1}{\frac{f \cdot x}{2 \cdot \rho} + \frac{1}{U_{co}}}$$
 (2.15)

With:

f = friction coefficient [-] Q = discharge  $[m^3/s]$ 

 $U_{c0}$  = velocity at the start of the dike crest [m/s]

#### 2.2.5. Landward slope dike

The *green water* overtopping flows down the inner slope of the dike. This is what causes erosion of the grass cover and it is therefore crucial to have a clear description of the flow. There have been several analytical solutions provided. They are presented below.

2.2. Flow description 13

Schüttrumpf provides an iterative analytical solution (equation 2.16), based on the continuity and momentum equations (Schüttrumpf and Oumeraci, 2005). A full derivation of this formula can be found in Schüttrumpf (2001). See figure 2.2 for definitions.

$$v = \frac{v_0 + \frac{k_1 \cdot h}{f} \cdot \tanh(\frac{k_1 \cdot t}{2})}{1 + \frac{f \cdot v_0}{h \cdot k_1} \cdot \tanh(\frac{k_1 \cdot t}{2})}$$
(2.16)

With:

$$t \approx -\frac{v_0}{g \cdot \sin\beta} + \sqrt{\frac{v^2}{g^2 \cdot \sin^2\beta} + \frac{2 \cdot s}{g \cdot \sin\beta}}$$
 (2.17)

And:

$$k_1 = \sqrt{\frac{2 \cdot f \cdot g \cdot \sin\beta}{h}} \tag{2.18}$$

The first step of the iteration can be approximated by:

$$h = \frac{v_0 \cdot h_0}{v} \tag{2.19}$$

With:

 $v_0$  = overtopping velocity at beginning of the landward slope ( $s_B=0$ )  $h_0$  = layer thickness at beginning of the landward slope ( $s_B=0$ )  $\beta$  = inner slope angle

f = bottom friction coefficient

Van Gent provides an analytical solution (equation 2.20), based on the continuity and momentum equation. A full derivation of this formula can be found in Van Gent (2002). See figure 2.2 for definitions. Differences between the solutions for the equations of Schüttrumpf and Van Gent are small and there are no differences for the maximum overtopping velocity on the landward slope for  $S_B \to \infty$  (Van Gent and Schüttrumpf, 2004). As the difference between methods are small or none the method of Van Gent is preferable because it requires no iterations and is thus easier to use in practise.

$$u_{B,2\%} = \frac{k_2}{k_2} + k_4 \cdot exp(-3 \cdot k_2 \cdot k_3^2 \cdot s_B)$$
 (2.20)

With:

$$k_2 = \sqrt[3]{g \cdot \sin\beta} \tag{2.21}$$

$$k_3 = \sqrt[3]{\frac{1}{2} \frac{f}{h_{0,2\%} \cdot u_{0,2\%}}}$$
 (2.22)

$$k_4 = u_{0,2\%} - \frac{k_2}{k_3} \tag{2.23}$$

With:

 $u_{0,2\%}$  = overtopping velocity at beginning of the landward slope ( $s_B=0$ )  $h_{0,2\%}$  = layer thickness at beginning of the landward slope ( $s_B=0$ )  $\beta$  = inner slope angle

f = bottom friction coefficient

For the remainder of this report it is important to understand what kind of flow behaviour is predicted by equation 2.20. This is shown in the intermezzo below.

14 2. Overtopping

#### Extended analysis equation 2.20

A closer look at the equation already reveals a lot about how the function behaves. The one variable that changes (along the dike section) is the parameter  $s_B$ . The parameter  $s_B$  describes the distance along the slope of the dike. The  $s_B$  parameter is located inside the exponential. This therefore suggest a function with an asymptotic increase or decrease. The equation's behaviour is featured using a simple example (see figure 2.3).

u0 [m/s] = 0.1, 0.5, 1 h0 [m] = 0.2, 0.5 f [-] = 1  $\phi$  = 1/3

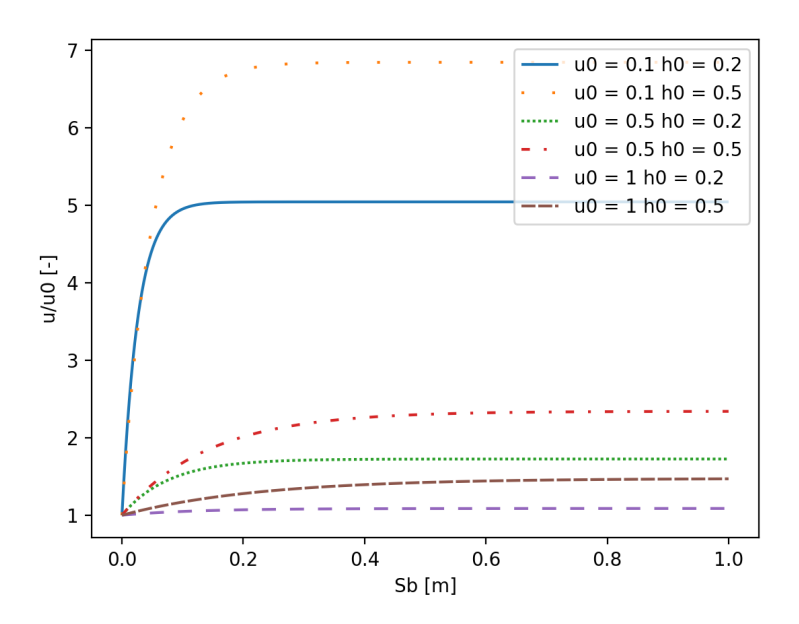


Figure 2.3: Flow behaviour predicted by equation 2.20 on lee side dike.

All examples show similar behaviour. As predicted the examples show a quick increase to a certain velocity, after which the flow velocity stabilizes.

Van Bergeijk provides an analytical solution (equation 2.24, see figure 2.4 for parameters) for the flow velocity at the inner slope of a dike, based on the one dimensional shallow water equation. The full derivation of this formula can be found in Van Bergeijk et al. (2019). The analytical model is limited to non-diffusive overtopping and the model is only valid for friction coefficients larger than the limiting friction coefficient (equation 2.29, Van Bergeijk et al., 2019).

$$U(s) = \frac{\alpha}{\beta} + \mu \cdot exp(-3 \cdot \alpha \cdot \beta^2 \cdot s)$$
 (2.24)

And:

$$\mu = U_{s,0} - \frac{\alpha}{\beta} \tag{2.25}$$

$$\alpha = \sqrt[3]{g \cdot \sin\phi} \tag{2.26}$$

$$\beta = \sqrt[3]{\frac{f}{2 \cdot Q}} \tag{2.27}$$

$$s = \frac{(x - B_c)}{\cos \phi} \tag{2.28}$$

$$f_{lim} = \frac{g \cdot Q \cdot sin(\phi)}{4 \cdot U_{s,0}^3} \tag{2.29}$$

With:

 $U_S$ , 0 = overtopping velocity at beginning of the landward slope ( $s_B = 0$ ) Q = discharge  $\phi$  = slope angle f = bottom friction coefficient

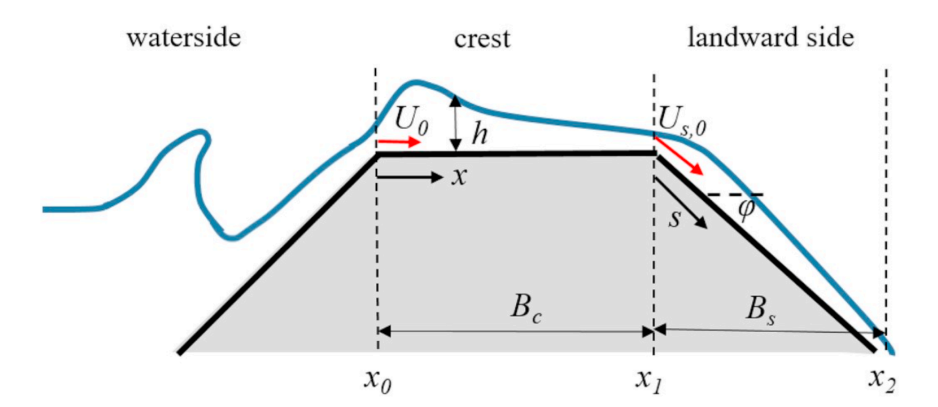


Figure 2.4: Schematic dike cross section(Van Bergeijk et al., 2019).

#### 2.3. Erosion due to overtopping

So far only overtopping in terms of flow is discussed. In the following subsections the overtopping in terms of flow is coupled to the occurrence of erosion. Both methods that are discussed do not replace the current maximum overtopping method but have a supportive role.

#### 2.3.1. Cumulative overload method

The cumulative hydraulic load is an erosional index for the grass cover of the inner slope, it is based upon the shear stress with threshold theory (Hoffmans et al., 2008). The shear stress with threshold theory introduces a critical velocity that is to be exceeded before any erosion can occur. For the cumulative hydraulic load is assumed that the duration of the overtopping load is less important. This is because during overtopping the wavefront rushes over the surface with large velocity, where the flow velocity increases to its maximum speed very fast. The grass cover experiences this as a kind of "impact" and this so-called impact is what causes the initiation or further development of erosion (Van Der Meer et al., 2010). The cumulative hydraulic load or cumulative overload method results in formula 2.30. This formula is tested and calibrated (Steendam et al., 2015) using the overtopping simulator (Van der Meer et al., 2006).

$$\sum (u^2 - u_c^2) \tag{2.30}$$

The correct critical velocity is not easily determined. A grass cover is not uniform, e.g. grass species, root density, length can vary and all have an impact on the critical velocity, hereby are the presence of trees, traffic signs etc. that weaken the grass cover not even considered. The *Schematiseringshandleiding grasbekleding* (2021) manual suggest for the run-up zone, considering grass on clay, a critical velocity of  $6.6\ m/s$  if the grass cover is closed and a critical velocity of  $4.3\ m/s$  if the grass cover is open. The manual does not provide a critical velocity value for the lee side of a dike. The critical velocity values provided by the manual for the run up zone will also be used for the lee side. Nonetheless, A site specific investigation needs to be done to determine and validate the correct critical velocity. It is important to realise, that because of the non uniformity of a grass cover the critical velocity can vary along the dike.

Table 2.6 provides threshold damage values according to Steendam et al. (2015). The *Schematiser-ingshandleiding grasbekleding* (2021) uses the "Failure" damage level in table 2.6 as critical damage level that is not to be exceeded.

16 2. Overtopping

Table 2.6: Cumulative overtopping damage levels (Steendam et al., 2015)

Initial damage	$\Sigma(U^2 - U_c^2) = 1000 \ m^2/s^2$
	$\Sigma(U^2 - U_c^2) = 4000 \ m^2/s^2$
Failure	$\Sigma(U^2 - U_c^2) = 7000 \ m^2/s^2$

#### 2.3.2. Erosional equivalence

The erosional equivalence method (Dean et al., 2010) provides a cumulative work erosional index and is similar to the cumulative overload method. Both methods require a certain threshold value to be exceeded before any erosion occurs. The difference between both methods is that the cumulative overload method is based upon an excess of shear stress where the erosional equivalence method is bases upon an excess of work.

# Offshore boundary conditions

This chapter discusses the offshore [x=0] boundary condition for the SWASH WGD model. The offshore boundary consist of a JONSWAP [ $\gamma$  = 3.3] wave spectrum.

#### 3.1. Initial boundary conditions

For the design of the WGD Sweco used the program Hydra-NL to calculate hydraulic boundary conditions. Hydra-NL is a probabilistic model that calculates hydraulic loads, such as water level, wave conditions and overtopping to assess and design primary flood defences (Duits, 2020). The WGD is designed for a lifetime of 50 years and has an overall failure probability of 1/3000 (SWECO, 2021b). The maximum allowable overtopping criterion is set to 10 l/s/m and the overtopping failure mechanism has a maximum exceeding probability of 1/37500 years. The overtopping failure mechanism appeared normative for the crest height. The Hydra-NL calculation in which overtopping is predicted gives the expected wave conditions at the toe of the dike. These expected wave conditions are  $H_{\rm S}=2.33$  m,  $T_{m-1,0}=4.01$  s, angle of incidence (to dike normal) = 26°, water level = 7.99 m+NAP and the wind velocity (at 10 meters above water level surface) = 37.5 m/s .

The wave conditions at the toe of the dike are predicted by Hydra-NL as follows, wave data from the Nordsea is extrapolated using SWAN through the Waddensea, the Ems estuary and finally through the Dollard until the dike toe. Extrapolating wave data comes with inaccuracies and the extrapolated wave data should be carefully looked at. A closer look to the given wave data shows that the combined wave conditions are most likely physically not possible. The steepness criterion is violated, both the Kamphuis breaker criterion (Kamphuis, 1997, equation 3.2) as well as the Miche breaker criterion (Schiereck and Verhagen, 2012, equation 3.1) is violated, the waves are too steep to exist. Equation 3.1 gives the highest physically possible individual wave  $(H_b)$ , for irregular waves the highest significant wave height  $(H_s)$  is about half the  $H_b$  value.

A wave period  $(T_{m-1,0})$  of 4.01 s and a water depth of 6 m gives, following the dispersion relationship (Holthuijsen, 2007), a wave length of 23.2 m . This results in, using equation 3.1, an individual wave height  $(H_b)$  of 3.05 m, which is for irregular waves a significant wave height  $(H_s)$  of 1.53 m . This value for the significant wave height is far below the expected significant wave height of 2.33 m according to Hydra-NL. Thus, the combination of wave height and wave period predicted by Hydra is not possible.

$$H_b = 0.142 \cdot L \cdot \tanh\left(\frac{2\pi}{I} \cdot d\right) \tag{3.1}$$

With:

 $H_b$  = individual wave height [m] L = wave length [m] d = depth [m]

$$H_s = L_p \cdot 0.095 \cdot e^{4 \cdot \alpha} \cdot \tanh(\frac{2\pi d}{L_p})$$
(3.2)

With:

```
H_s = significant wave height [m] L_p = wave length of breaking waves calculated using the peak period [m] d = depth [m] \alpha = slope [-]
```

The Hydra-NL wave conditions ( $H_{\rm S}=2.33$  m,  $T_{m-1,0}=4.01$ ) being physically not possible poses a problem. This essentially means that these wave conditions will never occur. Let us model these wave conditions for argument sake. The foreshore is considered intermediate water depth and therefore included in the model. Figure 3.1 shows the variance energy density spectrum at start of the headland(seaside) and dike toe for these wave conditions. And as expected, there is a lot of energy dissipation, because the larger waves immediately break. The waves being physically impossible raises the question of what wave conditions should be used as boundary condition.

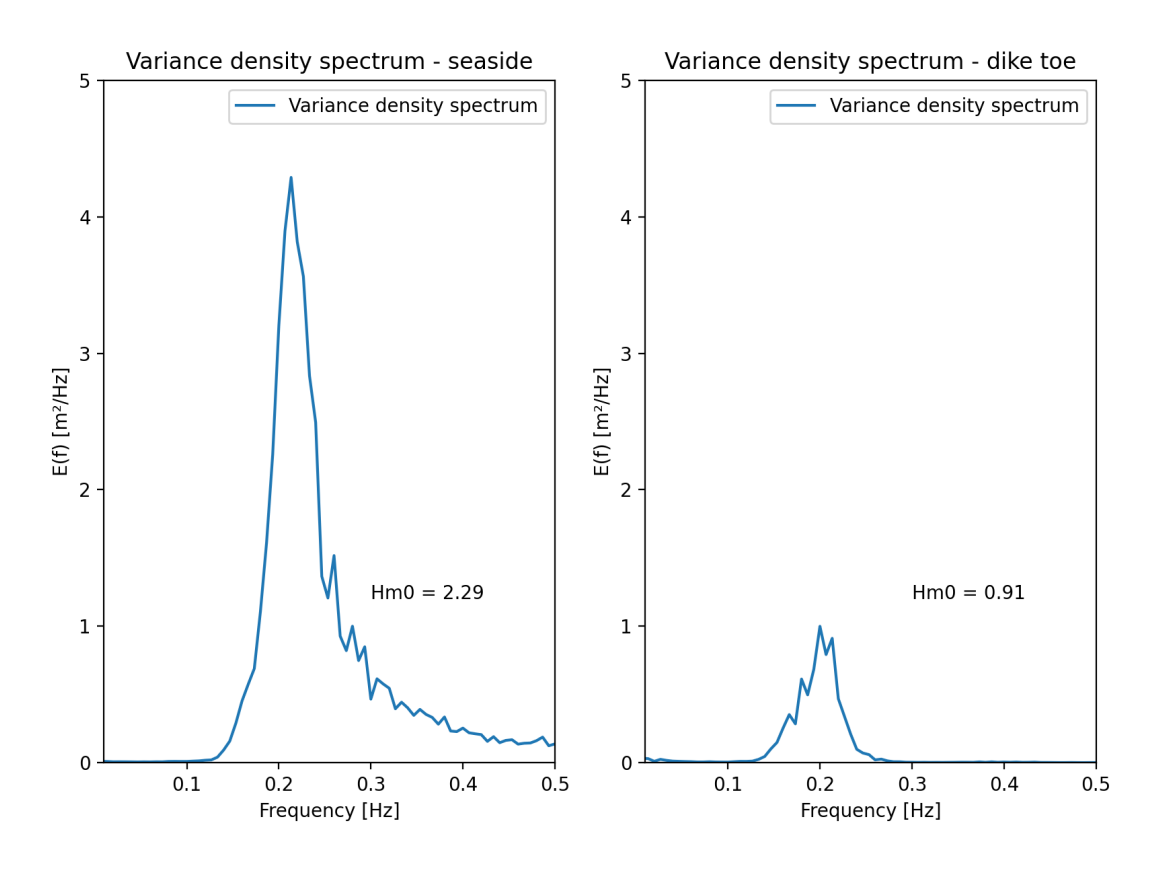


Figure 3.1: Variance density spectrum, left figure located at seaside[x=0], right figure located at dike toe[x = 1000].

Below are three options discussed that could resolve the issue concerning the missing boundary condition.

- Option 1: Assume that Hydra-NL predicted the wave height and water level correct but underestimated the wave period. Consequently, finding a new wave period using the wave steepness relation (equation 3.1) that can actually physically exist for the given wave height and run simulation.
- Option 2: Assume that Hydra-NL predicted the water level correct but not the wave height nor wave period. Find using the wave steepness relation (equations 3.1), the overtopping equation (equation 2.1) and the dispersion relationship a combination of wave height and wave period that would result in 10 l/s/m overtopping and analyse the flow behaviour on the lee side. This scenario would (for the WGD) quantitatively indicate whether 10 l/s/m of overtopping would result in flow velocities on the lee side that potentially could lead to erosion.

Option 3: The initial wave conditions (by Hydra-NL) are extrapolated (SWAN) through the Waddesea, the Ems estuary and finally though the Dollard until the dike toe. However, the sinuous shape of the Ems estuary makes it arguable whether waves that are not generated inside the Dollard are able to reach the dike. It is assumed that the waves are not able to travel through the estuary and are therefore locally generated. An empirical wind based wave generation formula is applied to find wave conditions at seaside boundary.

The sinuous shape of the Ems estuary makes it arguable whether waves that are not generated inside the Dollard are able to reach the dike. Therefore option 3 is considered the most likely. All options are simulated but only option 3 is elaborated in this report.

#### 3.2. Final boundary conditions

This section determines the wave conditions at the toe of the dike and the WGD model offshore boundary condition. The computational model used in this thesis (SWASH) can generate waves that are either regular or irregular. The goal of the computation is to retrieve the amount of overtopping (q), defined in section 4.2.4 , which is a parameter that represents an average. It therefore makes sense to use irregular waves at the boundary. Hydra-NL gives the water level [m], wave height [ $h_s$ ], wave period [ $T_{m-1,0}$ ] and wind conditions [m/s at 10m above water surface] at the toe of the dike for design conditions.

The design wind velocity is 37.5 m/s [at 10 m above water surface]. Figure 3.2 shows the bathymetry of the Dollard. Figure 3.2 combined with the design water level of 7.99 m+NAP gives a water depth of 8 m. This results in a dimensionless depth (equation 3.3) of  $\tilde{d} = \frac{9.81 \cdot 8}{37.5^2} = 0.56$ .

$$\tilde{d} = \frac{g \cdot d}{U_{10}^2} \tag{3.3}$$

With:

 $\tilde{d}$  = dimensionless depth [-]

g = gravitational acceleration constant  $[m/s^2]$ 

d = depth [m]

 $U_{10}$  = wind velocity at 10 meters above water surface [m/s]

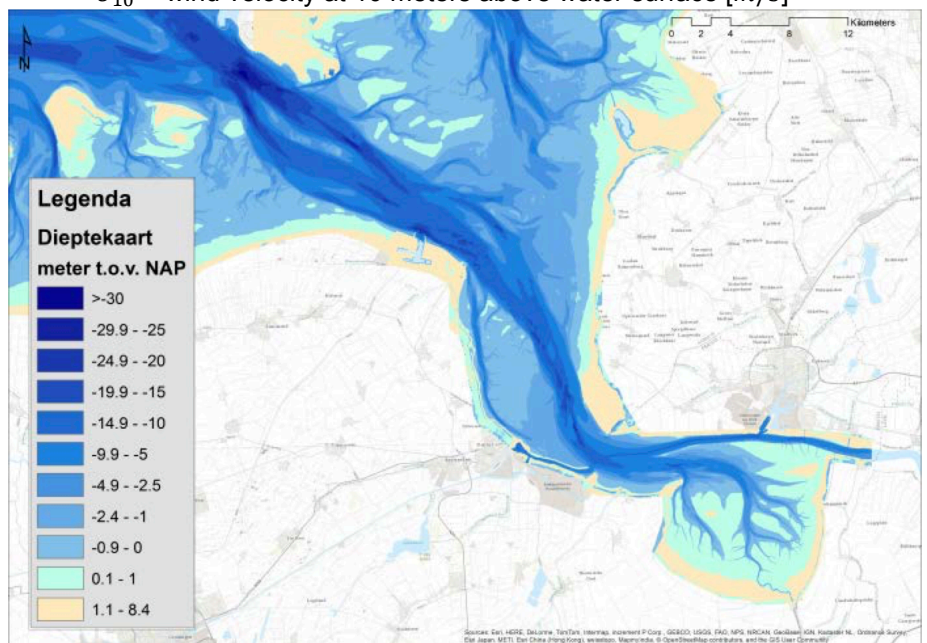


Figure 3.2: Bathymetry Dollard, legend shows depth in m with respect to NAP (Ysebaert et al., 2016). The maximum possible fetch is 9500 m. This results in a dimensionless fetch (equation 3.4) of  $\tilde{F} = \frac{9.81 \cdot 9500}{37.5^2} = 66.3$ .

$$\tilde{F} = \frac{g \cdot F}{U_{10}^2} \tag{3.4}$$

With:

 $\tilde{F}$  = dimensionless fetch [-]

g = gravitational acceleration constant  $[m/s^2]$ 

F = fetch [m]

 $U_{10}$  = wind velocity at 10 meters above water surface [m/s]

Respectively equations 3.5 and 3.6 give the dimensionless wave height and dimensionless wave period for all water depths using the dimensionless fetch and dimensionless water depth (Holthuijsen, 2007). The corresponding growth curves for these equations is presented in figure 3.3. Figure 3.3 combined with the dimensionless fetch and dimensionless water depth results in a dimensionless wave height of 0.015 and a dimensionless wave period of 1.1 . Equation 3.7 and equation 3.8 give respectively, the maximum significant wave height and maximum peak wave period. Resulting in a maximum wave height of  $H_{m0} = 0.015 \cdot \frac{37.5^2}{9.81} = 2.15$  m and a maximum period of  $T_{peak} = 1.1 \cdot \frac{37.5}{9.81} = 4.2$ .

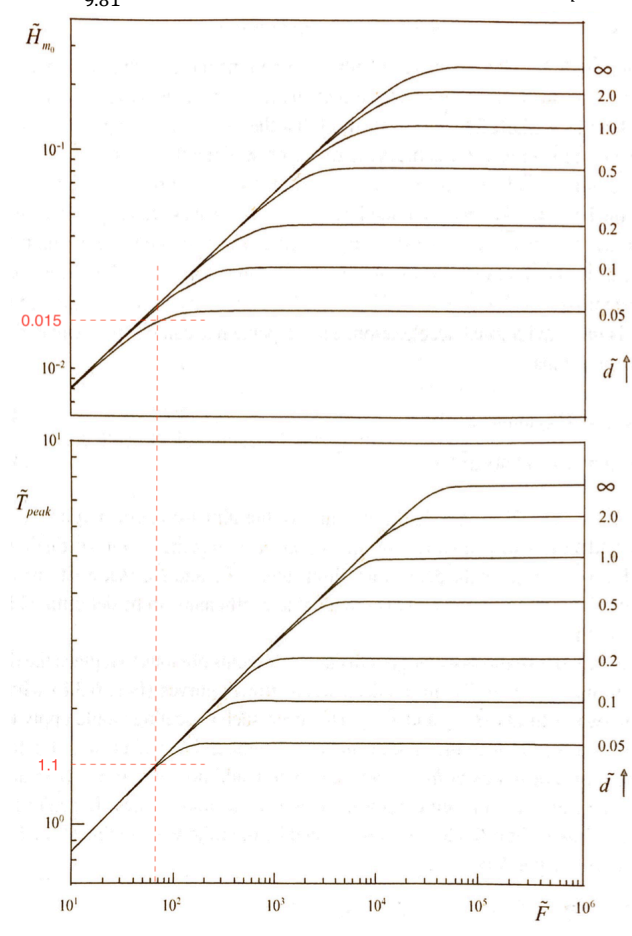


Figure 3.3: The dimensionless significant wave height(upper graph) and period(lower graph) as a function of dimensionless fetch (horizontal axes) and depth (vertical axes) (Holthuijsen, 2007).

$$\tilde{H} = \tilde{H}_{\infty} \left[ \tanh \left( k_3 \tilde{d}^{m_3} \right) \cdot \tanh \left( \frac{k_1 \tilde{F}^{m_1}}{\tanh k_3 \tilde{d}^{m_3}} \right) \right]^p \tag{3.5}$$

$$\tilde{T} = \tilde{T}_{\infty} \left[ \tanh \left( k_4 \tilde{d}^{m_4} \right) \cdot \tanh \left( \frac{k_2 \tilde{F}^{m_2}}{\tanh k_4 \tilde{d}^{m_4}} \right) \right]^q \tag{3.6}$$

With:

 $\tilde{H}$  = dimensionless wave height [-]  $\tilde{T}$  = dimensionless wave period [-]  $\tilde{H}_{\infty}$  = 0.24 [-]  $\tilde{T}_{\infty} = 7.69 \, [-]$  $\tilde{F}$  = dimensionless fetch [-]  $\tilde{d}$  = dimensionless depth [-]  $k_1 = 4.41 \cot 10^{-4} [-]$  $k_2 = 2.77 \cot 10^{-7}$  [-]  $k_3 = 0.343$  [-]  $k_4 = 0.1 [-]$  $m_1 = 0.79$  [-]  $m_2 = 1.45 [-]$  $m_3 = 1.14$  [-]  $m_4$  = 2.01 [-] p = 0.572 [-] q = 0.187 [-]

$$\tilde{H}_{m_0} = \frac{g \cdot H_{m_0}}{U_{10}^2} \tag{3.7}$$

With:

 $\tilde{H_{m_0}}$  = dimensionless wave height [-]  $g = gravitational acceleration constant [m/s^2]$  $H_{m_0}$  = wave height [m]  $U_{10}$  = wind velocity at 10 meters above water surface [m/s]  $\tilde{T}_{peak} = \frac{g \cdot T_{peak}}{U_{10}}$ 

(3.8)

With:

 $T_{peak}$  = dimensionless wave period [-]  $g = \text{gravitational acceleration constant } [m/s^2]$  $H_{peak}$  = wave period [m]  $U_{10}$  = wind velocity at 10 meters above water surface [m/s]

The empirical wind based wave generation calculation concluded that a maximum significant wave height of 2.15 m was possible or waves with a peak period of 4.2 s. A combination of the 2.15 m significant wave height with the 4.2 s maximum peak period is not possible according to the Miche wave steepness criterion. The Miche steepness criterion (equation 3.1) is used to find a matching wave period for the derived wave height and to find a matching wave height for the derived wave period. The empirical wind based wave generation formula derived a maximum wave height of 2.15, which gives according to Miche a wave period that is larger than the upper limit wave peak period by the empirical wind based wave generation formula of 4.2 s. This wave height/wave period combination is therefore disregarded. A matching significant wave height to the peak wave period of 4.2 s is 1.4 m.

Concluding, the waves at the toe of the dike should be a JONSWAP [ $\gamma = 3.3$ ] spectrum with  $H_s = 1.4$ m and  $T_{peak} = 4.2$  s. Given these waves the headland in front of the dike is considered deep water and will therefore not be included in the WGD computational model. It follows that the seaside boundary is located just in front of the toe of the dike and that the  $H_s = 1.4$  m and  $T_{peak} = 4.2$  s wave conditions are also the boundary condition for the WGD model.

The waves arrive at the dike with  $H_s=1.4$  m and  $T_{peak}=4.2$  m. This results in an Iribarren breaker parameter of  $\xi=\frac{1/7}{\left|\frac{H_s}{L_s}\right|}=0.63$ , which is in the plunging breaker regime (0.5 <  $\xi$  < 3, Schiereck

and Verhagen, 2012). The breakers being in the plunging breaker regime cannot be ignored as the computational model is a depth integrated model, this is elaborated on in section 4.2.3.

# 4

### **SWASH**

SWASH is a general-purpose numerical tool for simulating non-hydrostatic, free-surface, rotational flows and transport phenomena in one, two or three dimensions. The governing equations are the nonlinear shallow water equation including non-hydrostatic pressure and some transport equations (TU-Delft, 2021).

In this report SWASH is used to analyse 2D wave interactions from nearshore along a shallow foreshore to a sea dike. This wave path can be subdivided into two parts. Wave propagation from nearshore to a shallow foreshore and from a shallow foreshore to the sea dike.

De Roo et al. (2015) compared three numerical models to assess their performance considering 2D wave transformation processes from nearshore to a shallow foreshore. They compared SWASH, MIKE21 BW (a phase resolving Boussinesq wave model) and XBeach (a coupled phase-averaged spectral wave model for sea-swell and non linear shallow water model for infragravity waves), with physical data. De Roo et al. (2015) concluded SWASH was the preferred model showing high performance and being computational the most robust.

Gruwez et al. (2020) compared three numerical models to assess their performance considering wave interactions (e.g. overtopping) with sea dikes on shallow foreshores. They compared OpenFOAM (Reynolds-averaged Navier-Stokes equations solver), DualSPHysics (weakly compressible smoothed particle hydrodynamics model) and SWASH with a large scale laboratory experiment. OpenFOAM and DualSPHysics are highly complicated models and take enormous computational costs, were SWASH is respectively a much more simplified model and takes significantly less computational cost. Gruwez et al. (2020) concluded that all three models got a performance rating of good to very good considering wave-sea dike interactions. OpenFoam has the highest performance but SWASH showed similar results.

These studies proof that SWASH is capable of simulating wave interactions from nearshore along a shallow foreshore to a sea dike. Showing high performance, being computational robust and not very computational demanding make it an efficient and effective model to analyse the flow behaviour on the WGD.

This chapter contains the following, SWASH validation, WGD model bathymetry, WGD model settings, SWASH limitations and the data post-processing.

#### 4.1. Verification SWASH

According to literature SWASH can be used for assessing overtopping flows (Gruwez et al., 2020), however it was not used for such gentle dike slopes up to now. To verify whether SWASH can assess overtopping flows on a gentle outer dike slope, SWASH is compared with physical model tests by Schüttrumpf et al. (2001) (test nr. 3105009). Besides this verification there are several parameters in the model settings that could influence the model. This section also contains a sensitivity analysis for the depmin parameter, break parameter and the number of layers in the vertical. For the sensitivity analysis data from test (nr. 31050009) by Schüttrumpf et al. (2001) is used.

24 4. SWASH

The test by Schüttrumpf were intended to gain more insight in the hydrodynamic processes on a dike during overtopping events. Data for this tests that is made available in Bosman (2007) is used. The tests have been carried out by Schüttrumpf (2001) and validated and extended by large scale model test in the Large Wave Flume or GWK (Großer Wellenkanal) in Hannover (Schüttrumpf et al., 2001). The flume has a total length of 324 m, a width of 5 m and a depth of 7 meter. The test set-up is shown in figure 4.1. Throughout the flume measuring devices that measure surface elevation, pressure, velocity, flow depth and discharge are installed. Figure 4.2 shows the locations of measuring devices on the crest and lee side of the test set-up. As the test set up is large scale, therefore no scale effects are present.

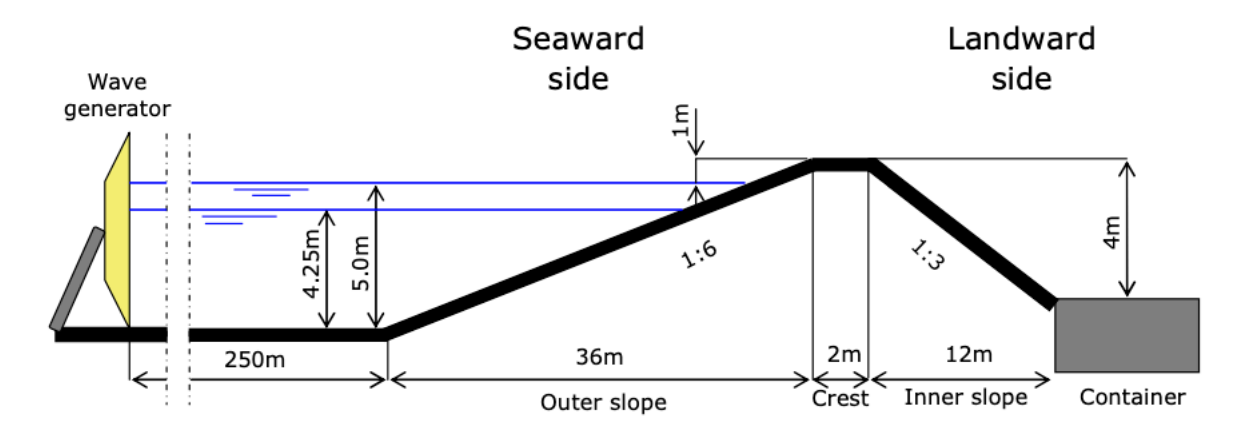


Figure 4.1: Physical model set-up GWK Hannover (Bosman, 2007).

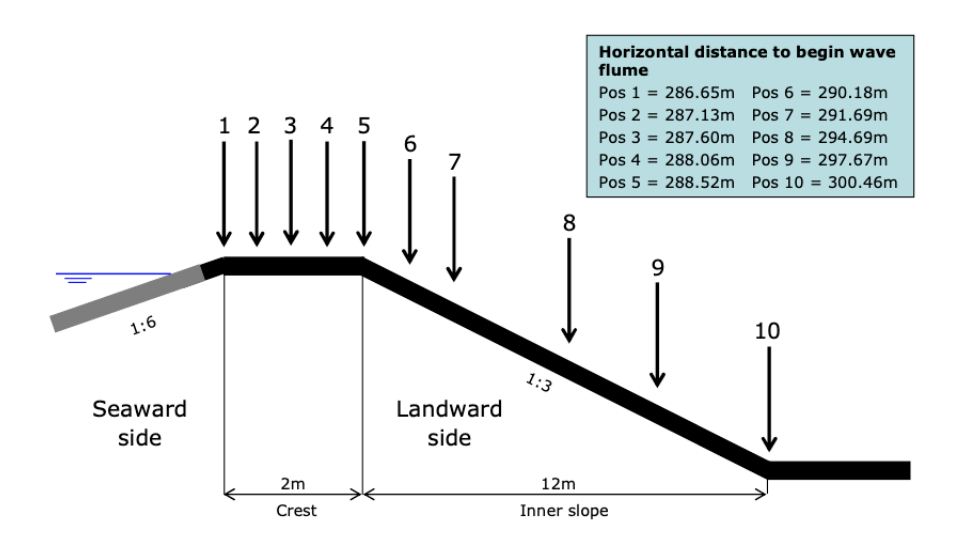


Figure 4.2: Shows the position of instruments that measure the flow velocity, pressure and flow depth (Bosman, 2007) for the tests by Schüttrumpf (Schüttrumpf et al., 2001).

#### 4.1.1. Set-up Schüttrumpf SWASH simulation

The SWASH set-up in terms of model settings of the Schüttrumpf simulation is similar to the WGD SWASH set-up. The computational domain is 2D, an x-axis perpendicular to the dike and 2 layers in the z-direction. The computational domain is 400 m in length and is subdivided by 4000 equally spaced cells. The bathymetry is build as shown in figure 4.1. The depth for which flooding and drying is checked is set to 0.0001 m. A water level of 4.99 m is set, giving a freeboard of 1.01 m. The right boundary (see figure 4.1) consist of a 100 m sponge layer and radiation boundary to optimize wave absorption. The left boundary(see figure 4.1) is where regular waves are generated. The height and period of these waves are 1.0 m and 7.5 s respectively. A cf = 0.018 manning friction coefficient is

4.1. Verification SWASH 25

used. Similar to the WGD SWASH set-up the simulation is non-hydrostatic, the command break is used to account for proper wave breaking and momentum is preserved. The CFL restriction is as follows,  $CFL_{High}$  = 0.5 and  $CFL_{Low}$  = 0.1 . Data (wave height [m], discharge [ $m^3/s/m$ ], velocity [m/s] and water layer thickness [m]) from the SWASH simulation is retrieved at the toe of the dike and at the same locations as in the original tests, see figure 4.2. The time step of the simulation is 0.0005 s and the total simulation duration is 8 minutes. The velocity measurements are retrieved with 0.1 s intervals. Due to the regular waves, a steady state condition is achieved quickly, therefore allowing for a relatively short simulation period.

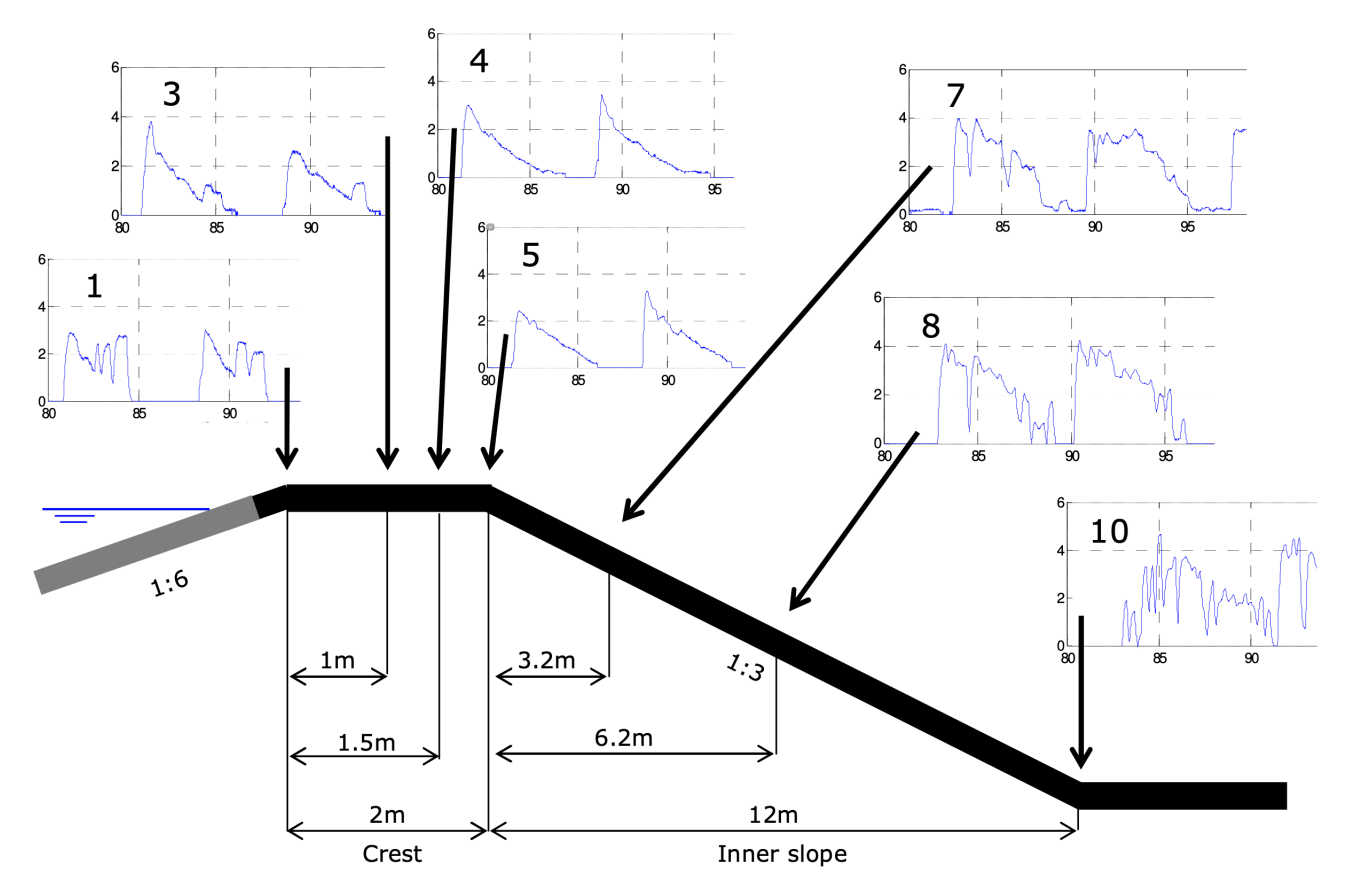


Figure 4.3: Data of test 31050009 (Schüttrumpf et al., 2001), regular waves H = 1.0 m, T = 7.5 s and  $R_c$  = 1.01 m. The data shows velocity measurements at the locations given in figure 4.2 (Bosman, 2007).

26 4. SWASH

#### 4.1.2. Breaker parameter

The scenarios discussed in this paper describe waves travelling from the deep sea to the shore and even until over the dike, wave breaking is an inevitable part of this process. A proper representation of energy dissipation due to wave breaking requires a vertical resolution of 10 - 20 layers. For lower resolutions (<5 vertical layers) the initiation of wave breaking is often delayed when compared to observations, and dissipation in the surf zone is underestimated (Smit et al., 2013). The SWASH model setups used in this paper all have a vertical resolution of 2 layers, in which wave breaking would thus be underestimated. However, SWASH included a method to resolve this issue. If initiated, SWASH uses the so called hydrostatic front approximation, which prescribes a hydrostatic pressure distribution around breaking waves. Whether a grid point is labelled for hydrostatic computation depends on a certain steepness criterion which is expressed in terms of the rate of surface rise,  $\partial_t \eta > \alpha c$  (Kennedy et al., 2000). Once labelled for hydrostatic pressure computation a point becomes non-hydrostatic again if the crest of the wave has passed. To represent the persistence of wave breaking the  $\alpha$  criterion is reduced to  $\beta$  if a neighbouring grid point has been labelled for hydrostatic computation,  $\partial_t \eta > \beta c$  (Smit et al., 2013).

Schüttrumpf et al. (2001) used regular waves H = 1 m and T = 7.5 s. The outer slope is 1:6. The period of 7.5 s results in a deep water wavelength of 87.8 m. This results in a wave steepness of 1.14%.

This results in an Iribarren parameter of  $\xi = \frac{\frac{1}{6}}{\sqrt{\frac{1}{87.8}}} = 1.56$ , which is in the plunging breaker regime

(Schiereck and Verhagen, 2012). The plunging waves of the WGD model have a wave steepness of 6.2%. The waves in the SWASH Schüttrumpf test are less steep than the waves of the WGD model, however the breaker type is similar.

To test the influence of  $\alpha$  and  $\beta$  on the simulation and to test which configuration of  $\alpha$  and  $\beta$  represents plunging waves best. The test set-up described in section 4.1.1 is repeated with different values for  $\alpha$  and  $\beta$ . Friction coefficient the same as for the WGD model (manning = 0.018) and with a depmin parameter of 0.0001 m.

All combinations of  $\alpha$  and  $\beta$  values shown in table 4.1 have been compared. The default setup appeared best and is shown in figure 4.4. Only the run with default settings is shown because of plot readability.

Figure 4.4 shows the flow velocity of the physical model test by Schüttrumpf and the SWASH results at the end of the crest (location 4, see figure 4.3). The SWASH model shows high accuracy considering the peak flow velocities and lower accuracy considering the lower trailing velocities. SWASH overestimates the trailing velocities. Given the fact that the inaccuracy is an overestimation instead of an underestimation would indicate that the model outcome is more conservative. Therefore, the overestimation of the trailing flow velocities is considered unfortunate but not a blocking issue for the outcome of this research.

Figure 4.5 shows the flow velocity of the physical model test by Schüttrumpf and the SWASH results halfway the lee side (location 7, see figure 4.3). The SWASH model shows the same peak velocities, the duration of the peak is shorter compared to the Schüttrumpf measurements. SWASH underestimates the duration of the peak. As the post processing only requires the peak velocity and not its duration, SWASH underestimating the duration of the peak is not considered very important.

The SWASH WGD and the SWASH Schüttrumpf model have the same breaker type. This tests shows that although the breaking waves are plunging and SWASH being a depth integrated model that due to the hydrostatic front approximation SWASH represents reality reasonably well. It provides confidence that SWASH simulates breaking waves in the WGD model reasonably.

4.1. Verification SWASH

Table 4.1: Table with alpha and beta values

	Run02(default)	Run00	Run01	Run03	Run04	Run05	Run06	Run07	Run08	Run09	Run10
α	0.6	0.8	1.0	0.8	0.4	0.4	0.6	0.8	0.4	0.6	0.8
β	0.3	0.4	0.5	0.3	0.3	0.2	0.2	0.2	0.1	0.1	0.1

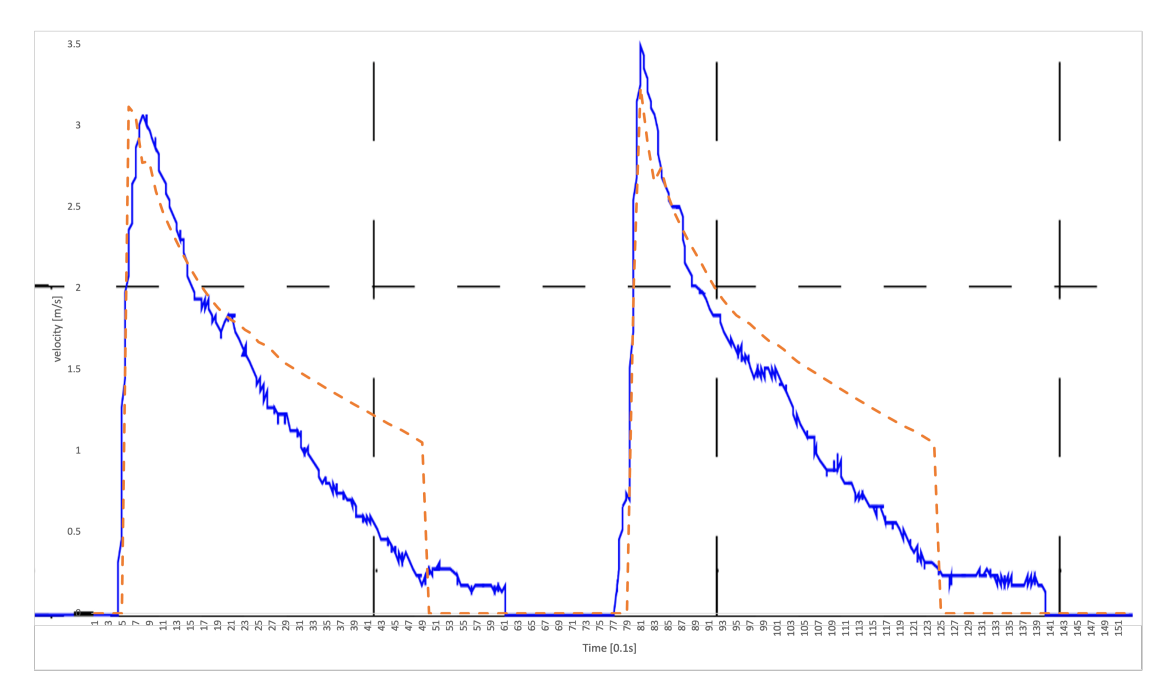


Figure 4.4: Plot showing Schüttrumpf data and SWASH results for run02 (default settings, see table 4.1), at location 4, which is at the end of the crest. The orange dotted line represents the SWASH simulation results and the continuous blue line represents the physical model results. The period of the SWASH waves seems to be shorter than the physical model results but this is because of the data post-processing.

28 4. SWASH

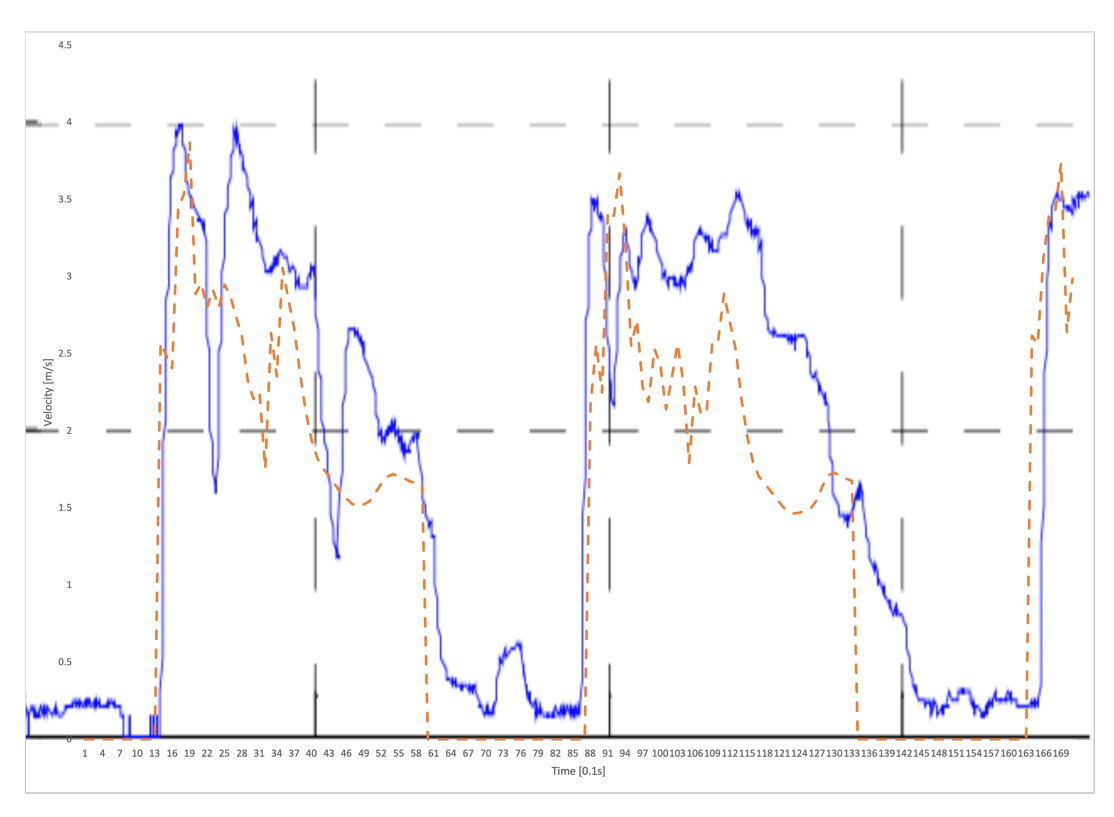


Figure 4.5: Plot showing Schüttrumpf data and SWASH results for run02 (default settings, see table 4.1), at location 7, which is halfway the lee side. The orange dotted line represents the SWASH simulation results and the continuous blue line represents the physical model results.

4.1. Verification SWASH 29

#### 4.1.3. Depmin parameter

For model stability reasons the depmin parameter is altered. The depmin parameter is the water depth for which flooding and drying is checked. Any water depth below the depmin depth is considered dry and kept out of the computation. The SWASH simulations discussed in this paper describe overtopping events including the flow over the crest and lee side of the dike. Consequently, there is a possibility of very small water depths. It is therefore not justifiable to simply and without consideration increase the depmin parameter to guarantee stability of the computation.

To test whether the depmin parameter is of importance, the test set-up described in section 4.1.1 is repeated with varying depmin parameter. During these computations friction is neglected. The depmin parameter configurations tested are 0.00005 m (default option), 0.01 m, 0.001 m and 0.0001 m. The SWASH computations are compared with the data presented in figure 4.3.

The default depmin value and both 0.01 m and 0.001 m provided similar results, they resulted in the peak flow velocity being somewhat underestimated. The depmin value of 0.0001 m showed slightly different results compared to the other three and predicted the peak flow velocity more accurately compared to the other configurations. The depmin configuration of 0.0001 m is therefore favourable over other configurations.

#### 4.1.4. Multiple layers

A simulation with a higher resolution in the vertical makes it significantly harder to maintain a stable simulation and the simulation time increases immensely. However, more vertical layers could have a significant influence on the simulation. For instance breaking, as mentioned previously, for <5 layers breaking is enhanced by the hydrostatic front approximation and for 10-20 layers all breaking is properly resolved without any approximations (Smit et al., 2013). Meaning the hydrostatic front approximation is not needed for 10-20 layers. To test the influence of a larger vertical resolution the simulation is repeated with a vertical resolution of 20 layers.

The test set up is as described in section 4.1.1 except for the break statement being disregarded. The friction is manning cf = 0.018 and the depmin value is 0.001 m (because of model stability).

Figure 4.6 displays the combined SWASH and Schüttrumpf results at the end of the crest (location 4, see figure 4.3). The SWASH results are represented by the blue dotted line. It is immediately clear that the flow velocities are highly overestimated and not very accurate. The SWASH simulations containing only two layers in the vertical combined with the break statement performed better. Concluding, a SWASH setup containing only two layers in the vertical combined with the break statement is preferential.

#### 4.1.5. Irregular waves

To validate whether SWASH predicts the amount of overtopping correct the Schüttrumpf test set-up is repeated with irregular waves and compared with the Eurotop overtopping equation (see equation 2.1, *Eurotop*, 2018). The SWASH settings are similar as for the previous simulation, except for the wave boundary condition. The wave boundary conditions is defined by a JONSWAP [ $\gamma = 3.3$ ] spectrum with  $H_{m0} = 0.9$  m and  $T_{peak} = 6.5$  s. This would results according to equation 2.1 in 14.9 l/s/m overtopping. The SWASH model measurements result in 12 l/s/m overtopping. SWASH slightly underestimates the amount of overtopping according to *Eurotop* (2018). The difference between SWASH and *Eurotop* (2018) is however small and considered negligible. The estimated overtopping by SWASH and *Eurotop* (2018) being rather similar provides confidence that SWASH predicts the overtopping in the WGD model rather accurate as well.

#### 4.1.6. Summary Schüttrumpf test

The default value for the breaker parameter showed compared to other breaker parameter settings best agreement with the psychical model test data. The SWASH WGD and the SWASH Schüttrumpf model have the same breaker type. This tests shows that although the breaking waves are plunging and SWASH being a depth integrated model that due to the hydrostatic front approximation SWASH represents reality very well. It provides confidence that SWASH simulates breaking waves in the WGD model accurately.

The depmin parameter is the water depth for which flooding and drying is checked. Any water depth

30 4. SWASH

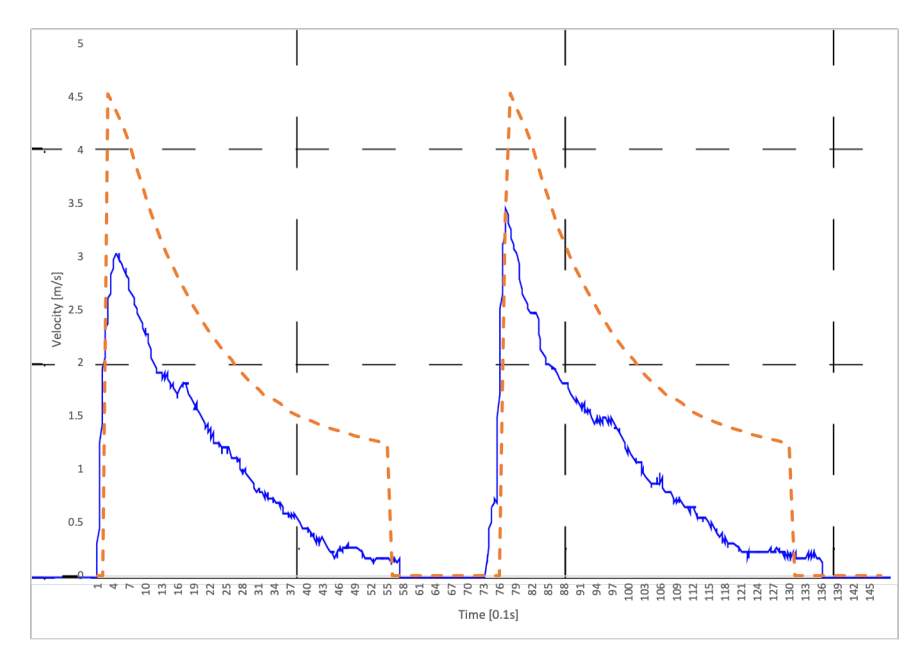


Figure 4.6: Location 4 (at the end of the crest), SWASH simulation with 20 layers in the vertical. The orange dotted line represents the SWASH simulation results and the continuous blue line represents the physical model results.

below the depmin depth is considered dry and kept out of the computation. The depmin configuration of 0.0001 m showed the highest model accuracy and is therefore favourable over other configurations. The computation with 20 layers in the vertical lead to longer a computational time, a less robust model and the results were worse than for the 2 layer simulation. The simulation with 20 layers is therefore disregarded as a practical option.

The simulation with irregular waves produced similar overtopping as predicted by the Eurotop overtopping equation. The estimated overtopping by SWASH and *Eurotop* (2018) being rather similar provides confidence that SWASH predicts the overtopping in the WGD model rather accurate as well.

#### 4.2. "Wide Green Dike" SWASH model

This section contains all important information about the SWASH WGD model. The bathymetry, model settings, model limitations (considering wave breaking) and the post processing is discussed.

#### 4.2.1. Bathymetry and dike geometry

The model domain is presented in figure 4.7. The bathymetry of the headland in front of the dike is retrieved from AHN ("ahn viewer", 2021) but is considered deep water and consequently not important for wave transformation and thus not included in the model. The bottom of the entire model is non porous and no sediment transport. The roughness coefficient is specified in the model settings (see section 4.2.2).

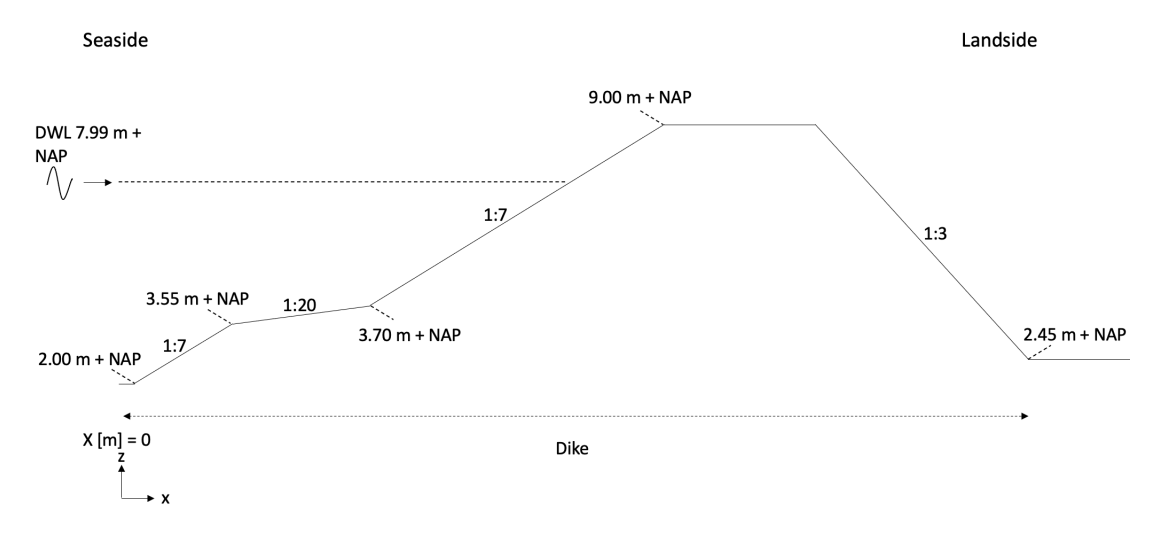


Figure 4.7: Schematic figure of computational domain. This figure shows all important dimensions but is not to scale.

#### 4.2.2. Model settings

The WGD is modelled in a 2-Dimensional computational domain (see figure 4.7). It includes an x-direction perpendicular to the dike and a z-direction in the vertical. It does not include a y-direction parallel to the dike. The x-direction consist of headland and dike. The computational model in x-direction has a total length of 284 m, consist of 2840 cells and has a grid size of 0.1 m. The z-direction contains 2 water layers, equally thick. The water depth is specified beforehand at 5.98 m. The minimal depth for checking flooding/drying is set to 0.0001 m. The dike is covered with grass and modelled with a roughness factor f = 0.01 (Steendam et al., 2012), which corresponds to a manning roughness coefficient of 0.018.

The WGD is modelled during storm conditions. This includes a fixed high mean water level and storm wave conditions entering the domain. The seaward boundary is where the waves are generated following a JONSWAP [ $\gamma$  = 3.3] spectrum, defined using the significant wave height [ $H_S$ ] and mean period [ $T_{m-1,0}$ ]. A ramp function is applied of 30 sec, to start up the simulation smoothly. The lee side boundary consist of a Sommerfeld radiation boundary and sponge layer, this to maximize wave absorption and allows for the flow to leave the domain.

If there are 10 or more water layers in the vertical SWASH simulates breaking accurately. If there are fewer layers applied SWASH underestimates the amount of energy dissipation(Smit et al., 2013). This can be corrected using the BREAK statement. This command initiates the central differences scheme for the horizontal advection terms. The BREAK command combined with momentum conservation in u and w direction accounts for breaking properly.

Furthermore, the model is set to nonhydrostatic using the Keller-box scheme (recommended for <5 water layers) for the vertical pressure gradient. For a robust solution the ILU preconditioner is used. As non linear processes such as wave breaking are important the maximum Courant number is set to 0.5 and the minimum Courant number is set to 0.1. The time step is 0.002 sec and simulation period is 1 hour. The simulation is repeated multiple times using a different seed for the random number generator.

#### 4.2.3. Model limitations considering wave breaking

The waves arrive at the toe with  $H_s=1.4$  m and  $T_{peak}=4.2$  s. This results in an Iribarren breaker parameter of  $\xi=\frac{1/7}{\sqrt{\frac{H_s}{L}}}=0.63$ , which is in the plunging breaker regime (0.5 <  $\xi$  < 3, Schiereck and

Verhagen, 2012). SWASH is a depth integrated model and consequently any configuration with more than two solids in the vertical direction cannot be applied (Suzuki et al., 2017). Therefore separation due to splash air-entertainment (e.g. plunging waves) are not represented in the model. However, Suzuki et al. (2017) compared the predicted energy dissipation due to plunging breakers by SWASH with actual physical model tests and concluded that SWASH represents the energy dissipation reasonable well due to the shock capturing feature and hydrostatic front approximation. The hydrostatic front approximation

32 4. SWASH

prescribes a hydrostatic pressure distribution around breaking waves. Whether a grid point is labelled for hydrostatic computation depends on a certain steepness criterion which is expressed in terms of the rate of surface rise,  $\partial_t \eta > \alpha c$  (Kennedy et al., 2000). Once labelled for hydrostatic pressure computation a point becomes non-hydrostatic again if the crest of the wave has passed. To represent the persistence of wave breaking the  $\alpha$  criterion is reduced to  $\beta$  if a neighbouring grid point has been labelled for hydrostatic computation,  $\partial_t \eta > \beta c$  (Smit et al., 2013). Concluding, both literature and the results from the SWASH validation (see section 4.1.2) provide confidence that, although the waves are of the plunging type, SWASH will predict the energy dissipation in the WGD model reasonably well.

#### 4.2.4. Overtopping parameter q

For the WGD simulation, the overtopping [q] SWASH measurement is retrieved at the beginning of the crest. The overtopping is given as a discharge  $[m^2/s]$ , the discharge is a function of the water layer thickness [m] and flow velocity [m/s]. The retrieved discharge  $[m^2/s]$  is converted to l/s/m. At this stage, the retrieved data for q is the instantaneous overtopping. But as q [l/s/m] is defined as the average overtopping rate, the retrieved data is averaged over the simulation period to give the average overtopping rate q [l/s/m].

#### 4.2.5. Post-processing

The instantaneous individual overtopping is retrieved at the start of the crest (location 1, see figure 4.8). In order to calculate the instantaneous individual overtopping, the flow depth [m] and flow velocity [m/s] are multiplied. A depth criterion of 0.01 m is applied as a threshold. If the overtopping depth is smaller than the threshold the overtopping is not counted as one overtopping event.

The flow velocity is analysed every 0.1 s at the locations in figure 4.8. A depth criterion of 0.01 m is applied as a threshold. If the water depth is smaller than the threshold the flow velocity is set to zero. At each of the locations the cumulative overtopping method is used to tests for erosion and potential failure. Furthermore, for each location a peak over threshold method combined with linear regression is applied to retrieve the  $u_{2\%}$  and  $h_{2\%}$  values.

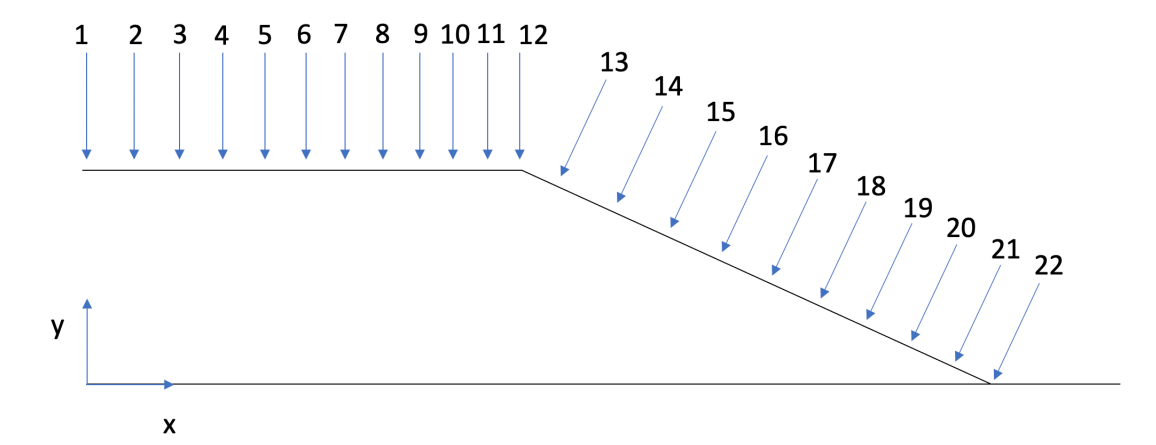


Figure 4.8: This figure indicates where the flow velocity is measured.

.

## Results

This chapter consist of two parts. It first discusses the results for the simulation with boundary conditions derived from the empirical wind based wave generation formula. It secondly zooms in on the flow behaviour on the crest and lee side of the WGD using different boundary conditions. The model domain is shown in figure 4.7.

#### 5.1. Results wind based wave conditions

The seaside boundary was represented by a JONSWAP [ $\gamma=3.3$ ] wave spectrum with  $H_s=1.4$  m and  $T_{peak}=4.2$  s. To validate whether SWASH has represented the boundary correctly the variance density spectrum is calculated. The water level is Fourier transformed to gain the wave variance density spectrum (see figure 5.1, Holthuijsen, 2007). The reliability of this Fourier transform is increased by means of quasi-ensemble averaging. Figure 5.1 shows the variance density spectrum at the toe. The variance density spectrum at the boundary displays a textbook JONSWAP spectrum with approximately the correct significant wave height and peak period.

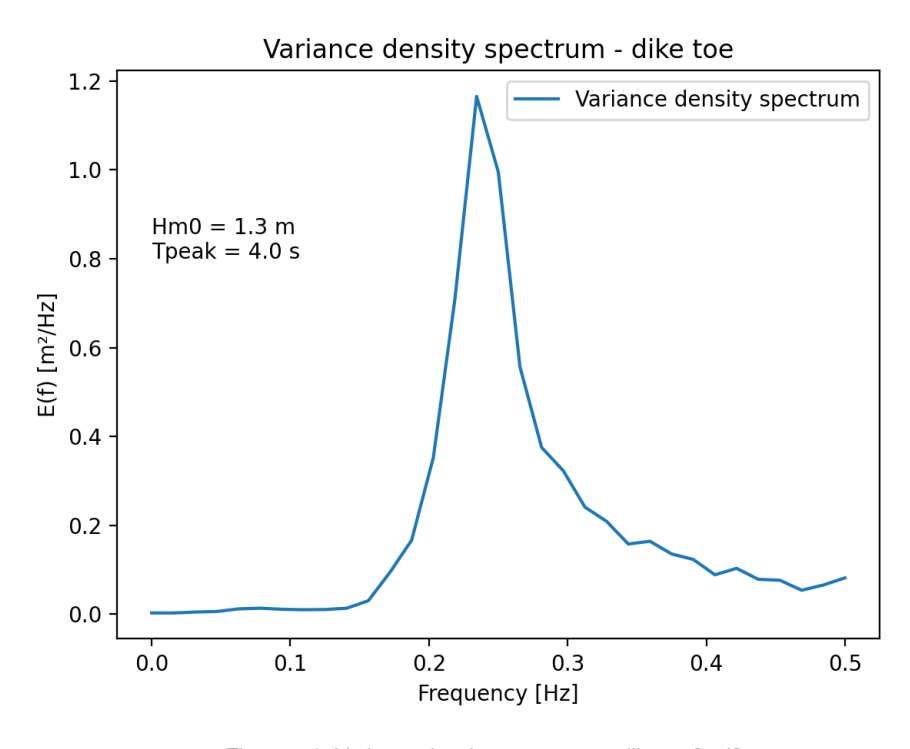


Figure 5.1: Variance density spectrum, at dike toe[x=0].

The WGD was modelled for 1 hour. During this hour, no single overtopping event was registered. The dike is designed for larger waves than the hydraulic boundary conditions of this simulation. So there being no or very little overtopping is as expected. Although the wave height being 10 cm off, there can be cautiously concluded that if the seaward boundary is determined by the locally generated waves determined of this thesis overtopping will not cause any erosion. Consequently the dike is safe. The overtopping failure criterion is normative for the crest height. As there is no erosion for design conditions the dike crest could be lower.

#### 5.2. Results of an extended analysis of flow velocity behaviour crest

The WGD project is a reinforcement project and consequently build on top of an existing dike. In the design phase is decided to keep the old dike the way it and to just put the clay of the new dike on top of the old dike. This means no excavation of the old dike. This results in the current crest width of 11 m. A crest width of 11 m is rather large with respect to other sea dikes. If the old dike would be excavated before realisation of the new dike the crest width could be shortened to 4 m instead of 11 m. It is interesting to highlight the effect of the crest on the flow velocity.

To examine the effect of the crest width on reducing flow velocities, the flow velocity (decrease) along the crest is analysed. The simulation described in section 4 is repeated with different boundary conditions. This resulted in three simulations. The boundary conditions are presented in table 5.1.

	Simulation	$H_{m0}$	$T_{m01}$	ξ
	1	2.02	5.47	0.76
	2	1.5	6	0.96
ĺ	3	0.9	6.82	1.41

Table 5.1: Different boundary conditions to analyse flow on crest, related to figure 5.2.

Figure 5.2 displays the results of the above mentioned three simulations. The results contain a  $u_{2\%}$  value on different locations on the crest retrieved by means of a peak over threshold method combined with linear regression. The figure displays the  $u_{2\%}$  on the y-axis normalised with the starting velocity versus on the x-axis the distance on the crest normalised with the total crest width (bc). The graph also displays the plotted equation by Van Gent for the crest. Here is the friction parameter used as a tuning parameter. The friction parameter f is  $f_{sim_1} = 0.055$ ,  $f_{sim_2} = 0.025$  and  $f_{sim_3} = 0.06$ , this corresponds for a water depth of 0.25 m with a manning coefficient (n) of  $n_{sim_1} = 0.042$ ,  $n_{sim_1} = 0.028$ ,  $n_{sim_1} = 0.043$  (Steendam et al., 2012). These manning friction coefficients are in the regime what is valid for grass (0.025 < n < 0.050, Chow, 1959). The tuning is based on the first initial flow velocity decrease. The figure also contains a vertical black line that indicates a 4 m crest width.

The results for the three simulations show similar behaviour. For all simulations the overall flow velocity decreases along the crest, however two phases can be identified. The simulations show a relatively large initial flow velocity decrease after which the flow velocity still decreases but only slightly. In other words, the intensity of the flow velocity decrease reduces. The flow velocity at the end of the crest is around 75%-80% of its initial velocity. It seems that the crest width only helps reducing the flow velocity efficiently to a certain extend. There can be argued that crest width should be wide enough to enable this first large velocity decrease, but making the crest wider is not a very efficient measure to reduce the flow velocity even more.

The equation by Van Gent expects a continuous flow velocity decrease towards the end of the crest. The equation predicts a large initial flow velocity decrease after which the intensity of the decrease reduces. This means that the equations behaves similar as the measurements show. Although the behaviour is similar the expected final velocity is very different. The Van Gent equation is fitted to the initial large flow velocity decrease. The difference is due to the second phase. The flow velocity measurements reduce far less than the Van Gent equation predicts. This causes the Van Gent equation to underestimate the flow velocity at the end of the crest and consequently also the flow velocities on the lee side.

As mentioned the vertical black line in the figure (see figure 5.2) indicates where the crest width is 4 meters. It is noteworthy that for all simulations the initial large decrease in flow velocity ends around

or just after this vertical black line. This means that the remaining crest width does not reduce the flow velocity very much and therefore a shorter crest would not cause the flow velocity on the lee side to increase very much. An extended analysis is needed to find the optimum crest width in terms flow velocity decrease, safety and costs but such an analysis is not included in this paper because it is out of scope.

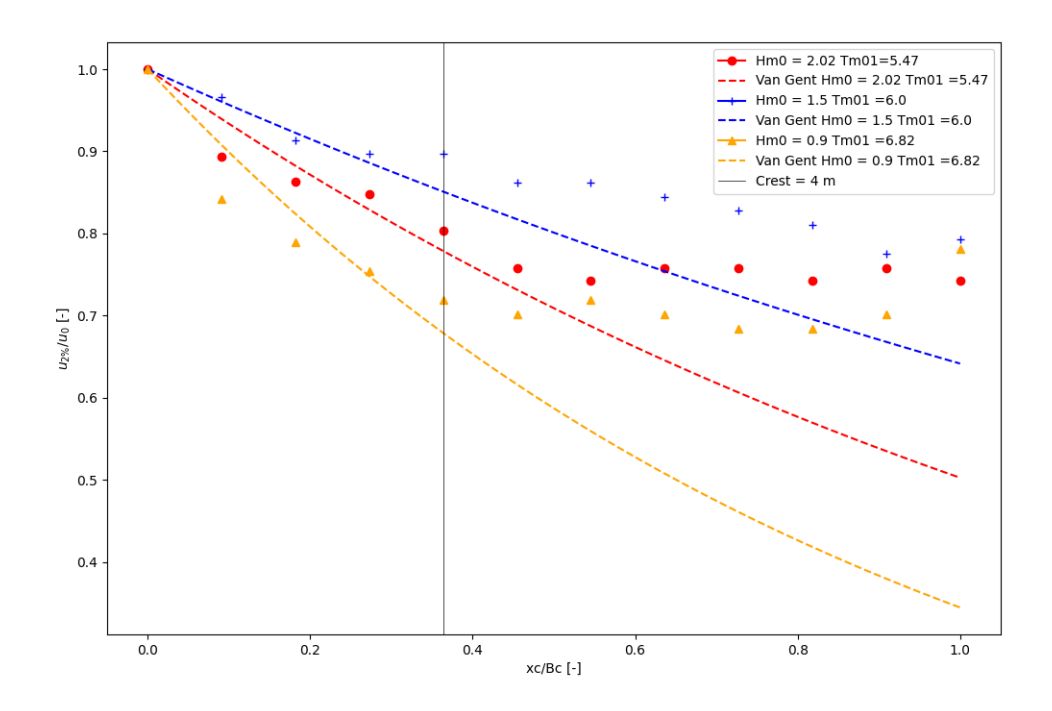


Figure 5.2: SWASH  $u_{2\%}$  measurements on crest for different wave height/ wave period combination. Accompanied by Van Gent equation for the crest for each wave height/ wave period combination. The y-axis displays the velocity[u] normalized by the initial velocity  $[u_0]$  at the start of the crest. The x-axis displays the position  $[x_c]$  on the crest normalized by the entire crest width  $[B_c]$ .

## 5.3. Results of an extended analysis of flow velocity behaviour lee side

The wave boundary condition provided by the empirical wind based wave generation formula resulted in no overtopping. It is off course trivial that the flow velocity on the lee side of the dike cannot be analysed if there is not a single overtopping event. This section uses a new random set of wave conditions that does generate overtopping such that the flow velocity on the lee side can be analysed.

The new hydraulic boundary conditions are the following,  $H_s = 2.02$  m and  $T_{mean} = 6.02$  s (see figure 5.3). The model setup and settings are the same for the simulation with the empirical wind based wave boundary conditions, the model settings and setup are described in chapter 4.

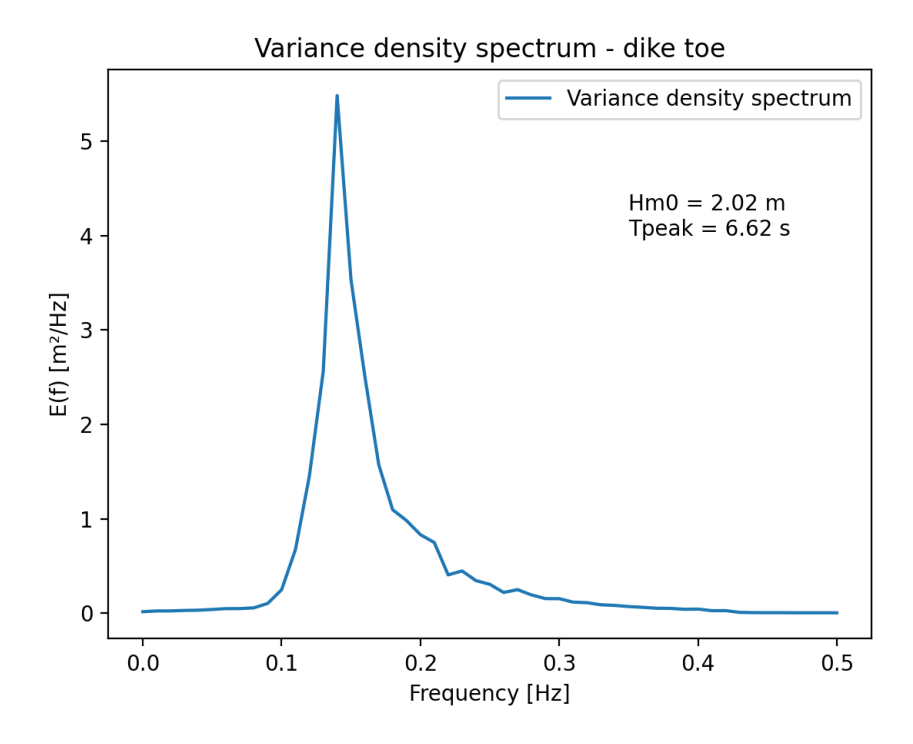


Figure 5.3: Variance density for boundary conditions  $H_s = 2.02$  m and  $T_{mean} = 6.02$ .

The simulation resulted in 57 l/s/m overtopping, which is almost 6 times larger than allowed, and would according to the 10 l/s/m criterion be destined to fail. The wave height/wave period combination would result in 65.8 l/s/m according to the *Eurotop* (2018) overtopping equation (equation 2.1). Meaning that SWASH slightly underestimates the amount of overtopping according to *Eurotop* (2018). Table 5.2 shows the cumulative overtopping method for the lee side for a 6 hour storm. According to Steendam et al. (2015) initial damage starts if the cumulative overload method reaches a value of 1000 and failure would occur if the cumulative overload method reaches a value of 7000. Table 5.2 shows that the cumulative overload value stays below a value of 7000 for every point along the lee side of the dike, meaning no failure of the dike. Van der Meer et al. (2015) uses 6.6 m/s as a critical flow velocity  $(u_c)$  for grass, which would results in no initiation of damage. If for some reason the  $u_c < 4.5$  m/s there is some initiation of damage at some locations along the lee side of the dike. But as there is no failure (or if  $u_c > 4.5$  m/s no initiation of damage) it most likely that the current correlation between overtopping [l/s/m] and failure is not correct.

Besides that there is no erosion on the lee side the table that presents the results for the cumulative overload method displays another interesting feature. Going from point to point along the dike slope the cumulative overtopping value first increases, but eventually decreases again. This essentially means that the flow velocity first increases but eventually decreases again. According to literature, elaborated on in section 2.2.5, the flow velocity would first increase and than stabilize but not decrease. That the results differ from literature is unexpected but interesting. The next section provides an extended analysis. For the extended analysis the  $u_{2\%}$  flow velocity is retrieved by means of the peak over threshold method combined with linear regression, this is shown for point 12 in figure 5.4 and 5.5.

Table 5.2: Results for cumulative overtopping method for points along the lee side of the dike (see figure 4.8) boundary conditions  $H_S = 2.02$  m and  $T_{mean} = 6.02$ 

Ucrit	Points									
[m/s]	13	14	15	16	17	18	19	20	21	22
3.0	3845	6063	6381	5907	4086	3183	2518	2563	2415	2462
3.5	2039	3912	4088	3603	2107	1020	557	356	205	165
4.0	543	2106	2434	2200	1036	343	145	59	25	1
4.5	85	655	1098	1098	438	96	21	0	0	0
5.0	0	134	264	506	184	8	0	0	0	0
5.5	0	8	38	177	77	0	0	0	0	0
6.0	0	0	0	6	25	0	0	0	0	0
6.5	0	0	0	0	0	0	0	0	0	0
6.6	0	0	0	0	0	0	0	0	0	0
7.0	0	0	0	0	0	0	0	0	0	0
7.5	0	0	0	0	0	0	0	0	0	0
8.0	0	0	0	0	0	0	0	0	0	0

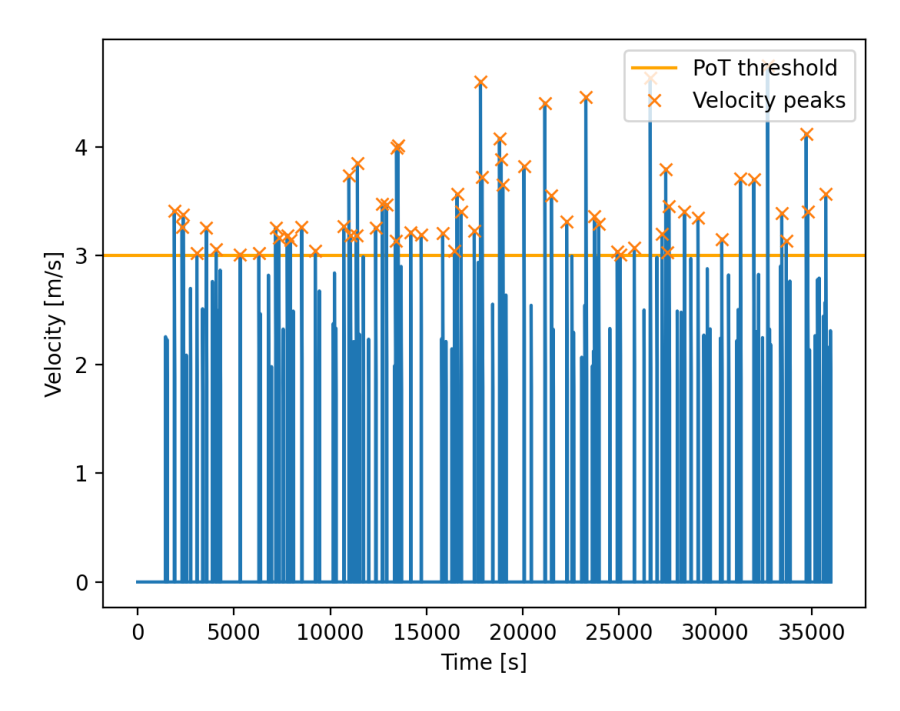


Figure 5.4: Peak over threshold, point 12

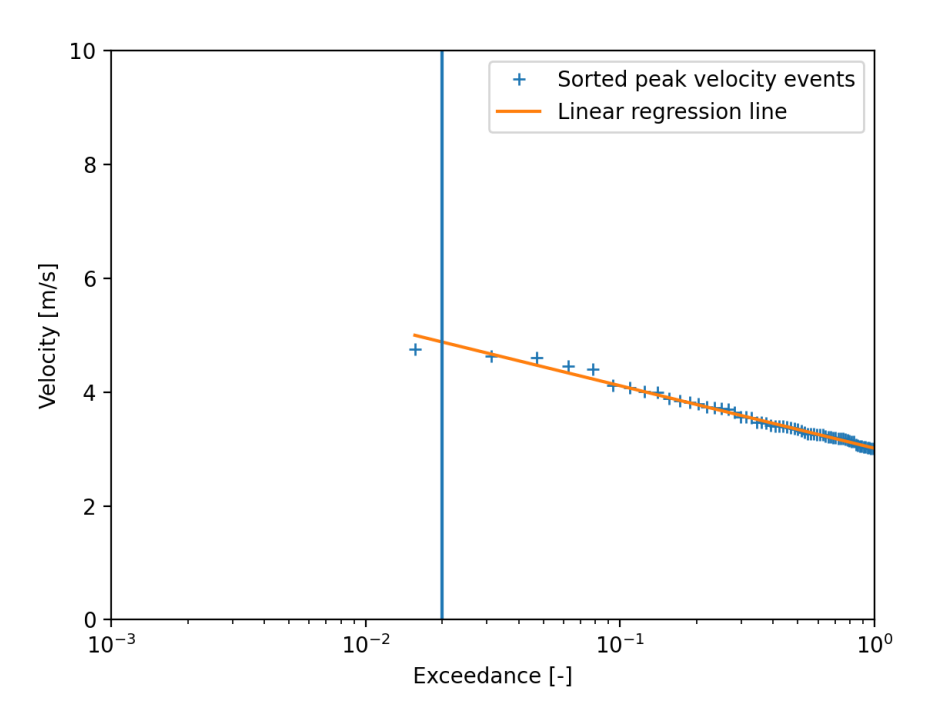


Figure 5.5: Exceedance point 12

#### 5.3.1. Kinematic Shock theory

The SWASH results show that the flow velocity on the lee side initially increases but also decreases again. The present day flow equations for the lee side describe the initial increase but not the observed decrease. To describe the flow velocity decrease kinematic wave theory is applied, which is widely used in modeling overland flows (Singh, 2017). The theory is first formulated by Lighthill and Whitham (1955) and states that there is a unique relation between discharge, concentration (depth) and position (Singh, 2017). Observation by Hughes and Nadal (2009) and Van Der Meer et al. (2010) indicate that the velocity profile of overtopping waves at the inner dike slope is shaped the same as the water elevation profile, which indicates that kinematic wave theory could possibly be applied because of the similar relation between u and h. The kinematic wave theory is based on the momentum balance between gravitation and bed friction, all other terms are neglected. This is possible because of the shallow character of the flow, with an horizontal extent in the order of 10 m and a vertical extend of 0.1 m

This section contains a formulation for the far field of the velocity on an inner dike slope. The theory of this section is provided by an informal memo from the chair of the thesis committee.

The formula is derived the following:

Mass Balance:

$$\frac{dh}{dt} + \frac{dhu}{dx} = 0 ag{5.1}$$

With:

h = water depth [m] u = flow velocity [m/s]

#### Momentum balance:

$$\frac{d}{dt}\rho uh + \frac{d}{dx}\frac{1}{2}\rho gh^2\cos a + \frac{d}{dx}\rho u^2h + \tau - \rho gh\sin a = 0$$
 (5.2)

With:

h = water depth [m] u = flow velocity [m/s]

g = gravittaional accelaration  $[m^2/s]$ 

 $\rho$  = density  $[kg/m^3]$ 

a = angle [-]

 $\tau$  = shear stress  $[kg/ms^2]$ 

Combined:

$$\frac{du}{dt} + g\cos a\frac{dh}{dx} + u\frac{du}{dx} + \frac{\tau}{\rho h} - g\sin a = 0$$
 (5.3)

#### **Assumptions:**

Steep slope

$$g\cos a = 0(g\sin a) \tag{5.4}$$

Shallow flow, derivatives  $\ll 1 = 0$ 

Reduced momentum balance:

$$c_f u^2 = gh \sin a \tag{5.5}$$

With:

 $c_f$  = friction constant [-]

or

$$u = \sqrt{\frac{h}{\beta}} \tag{5.6}$$

With:

$$\beta = \frac{c_f}{g \sin a} \tag{5.7}$$

The combined mass- and reduced momentum balance equation leads to a Burgers type equation:

$$\frac{dh}{dt} + \frac{3}{2}\beta^{-\frac{1}{2}}h^{\frac{1}{2}}\frac{dh^{\frac{3}{2}}}{dx} = 0$$
(5.8)

This equation (equation 5.8) resembles a wave equation which describes a travelling wave with celerity  $\frac{3}{2}\beta^{-\frac{1}{2}}h^{\frac{1}{2}}$ . The celerity contains depth and consequently the higher water levels will travel faster than the lower water levels such that the leading edge of the pulse will become deepest, and a shock develops. Due to mass conservation the wave profile upstream of the shock spreads out such that in time the wave becomes lower.

A solution for

$$h(t=0) = \delta(0)V \tag{5.9}$$

With:

V = volume  $[m^3]$ t = time [s]

x = distance along the dike inner slope [m]

ls:

$$h = \frac{4}{9}\beta \frac{x^2}{t^2} \tag{5.10}$$

Volume conservation can be used to obtain the shock position.

$$\int_0^{x_f} h dx = V \tag{5.11}$$

Results in:

$$x_f = \sqrt[3]{\frac{27}{4\beta}Vt^{\frac{2}{3}}} \tag{5.12}$$

The maximum velocity of the shock  $u_f$  is:

$$u_f = \frac{dx_f}{dt} = \sqrt[3]{\frac{2V}{\beta}} t^{-\frac{1}{3}}$$
 (5.13)

The maximum particle velocity in the shock  $u(x_f)$  is:

$$u = \sqrt{\frac{h(x_f)}{\beta}} = \frac{2}{3} \frac{x_f}{t} = \sqrt[3]{\frac{2V}{\beta}} t^{-\frac{1}{3}}$$
 (5.14)

Figure 5.6 is shown in chapter 2 but is shown again here as a reference to certain parameters. Especially parameter  $S_B$  is important which indicates the distance along the inner dike slope.

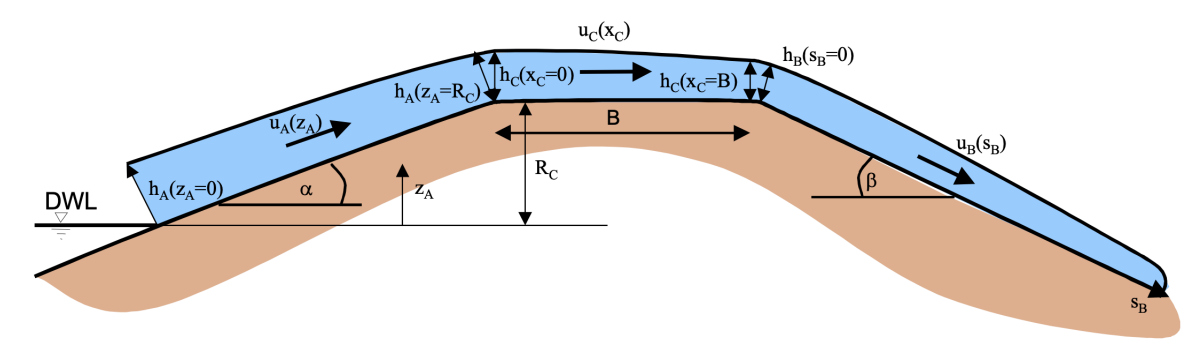


Figure 5.6: Schematic dike cross section defining parameters for equations Schüttrumpf and Van Gent (Van Gent and Schüttrumpf, 2004)

Figure 5.7 shows the  $u_{2\%}$  SWASH measurements (orange dots) for 10 locations on the lee side (see figure 4.8 measurement locations). As mentioned the  $u_{2\%}$  are retrieved by means of a peak over threshold method combined with linear regression. Following the orange dots it is clear that the flow velocity initially asymptotically increases, and after which it reaches some point it decreases again. The equation for the lee side by Van Gent is displayed by means of the blue dotted line. The parameters

 $u_0$  and  $h_0$  needed for this equation are retrieved at the end of the crest, which is point 12 in figure 4.8 . The equation by Van Gent predicts an asymptotic velocity increase after which it should stabilize. Comparing the Van Gent equation to the SWASH measurements it shows very good agreement to the first initial increase. But as the Van Gent equation does not predict any velocity decrease it shows no correspondence with the SWASH velocity measurement after they start to decrease.

The green line represents the shock theory equation (equation 5.13). The equation is only valid from the point where the velocity starts to decrease. This is why the function does not start at sb = 0. The volume parameter V is the volume at the point where the velocity starts to decrease, the volume is a function of velocity[m/s] and depth[m]. The velocity between points does not differ much hence the time parameter[t] is approximated by means of x/u. Comparing the Shock equation with the SWASH measurements it displays a very good agreement.

The friction coefficient for both equations is used as a tuning parameter and slightly varies for the Van Gent equation and the shock theory equation. The friction parameter f is  $f_{Van-Gent}=0.035$ , which corresponds to a manning friction coefficient of  $n_{Van-Gent}=0.036$  (Steendam et al., 2012). The friction parameter f is  $f_{Shock}=0.06$ , which corresponds to a manning friction coefficient of  $n_{Van-Gent}=0.047$  (Steendam et al., 2012). Both friction coefficients are within the regime what is valid for grass (0.025 < n < 0.050, Chow, 1959).

It seems that a combination of both formula can represent the flow velocity along the lee side of a dike.

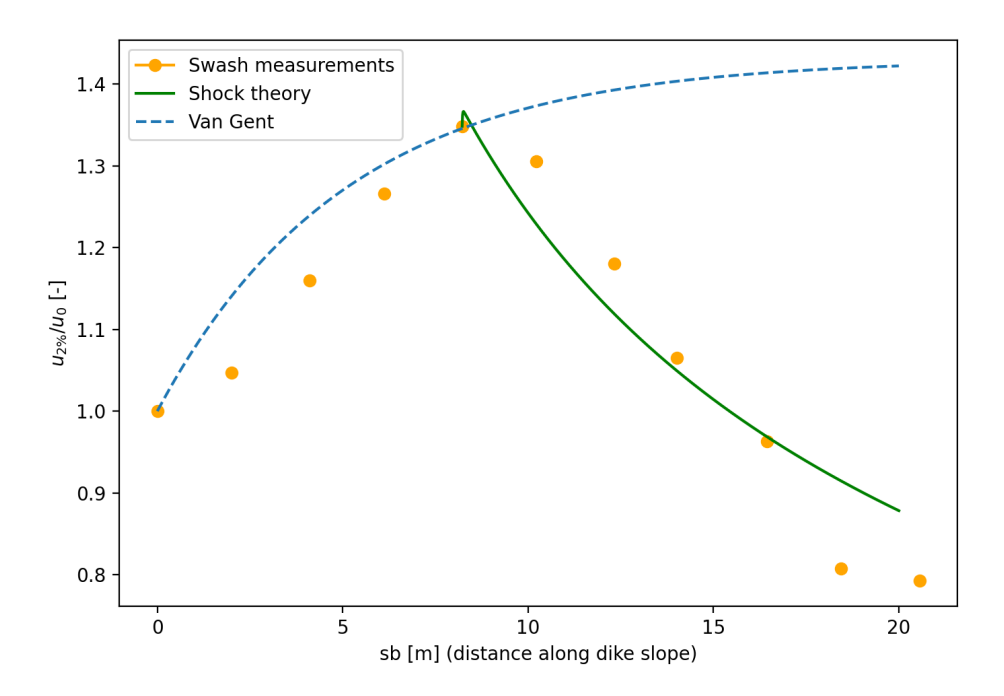


Figure 5.7: Plot showing  $u_{2\%}$  SWASH measurements, Van Gent equation for lee side and Shock theory. The y-axis displays the velocity on the lee side [u] normalized by the starting velocity [ $u_0$ ] at the end of the crest. The x-axis displays the position on the lee side of the dike.

Figure 5.7 shows the  $u_{2\%}$  SWASH measurements accompanied by the Van Gent and Shock theory lines. Figures 5.8, 5.9, 5.10,5.11, 5.12 and 5.13 show the SWASH measurements and accompanied Van Gent and Shock theory lines for individual waves. Figure 5.8 displays the highest wave (largest initial depth), figure 5.9 displays the lowest wave (lowest initial depth) and the other figures display another random wave (initial depth in between highest and lowest). For each simulation the friction coefficient is used as a tuning parameter and slightly vary for the Van Gent equation and the Shock theory equation. The friction coefficient (manning) for each simulation is shown in table 5.3. Also for individual waves it seems that a combination of both formula can represent the flow velocity along the lee side of a dike.

The graphs containing individual waves show similar behaviour to  $u_{2\%}$  (see figure 5.7). The SWASH measurements show an initial increase in velocity, after which it decreases again at some point. The equation by Van Gent shows good agreement with the initial increase but show no correspondence with the decrease in velocity. The Shock theory equation shows good agreement with the decrease in velocity. The tipping point is defined as the location on the dike slope where the velocity starts to decrease. The location of the tipping point is not the same for every wave but depends on the initial wave volume at the end of the crest. In figure 5.14 the x location of the tipping point based on the intersection between the Van Gent equation and Shock theory equation is plotted versus the initial wave velocity, depth and volume. Figure 5.14 shows that there is a linear relation between the location of the tipping point and depth, velocity and volume.

Another interesting feature is the following. In the graph containing individual waves there are also three horizontal lines included that display 100%, 97% and 95% of the final velocity predicted by the equation of Van Gent. It is interesting that for each graph the tipping point exactly or almost exactly coincides with the 97% line. So if the velocity increases to 97% of its predicted final velocity it starts to decrease and the Shock theory equation is valid.

Table 5.3: Manning friction coefficients for the Van Gent equation and shock theory equation in following figures (Steendam et al., 2012).

Figures	5.8	5.9	5.10	5.11	5.12	5.13
$n_{Van-Gent}$	0.040	0.036	0.039	0.038	0.037	0.034
$n_{shock}$	0.047	0.054	0.045	0.046	0.041	0.042

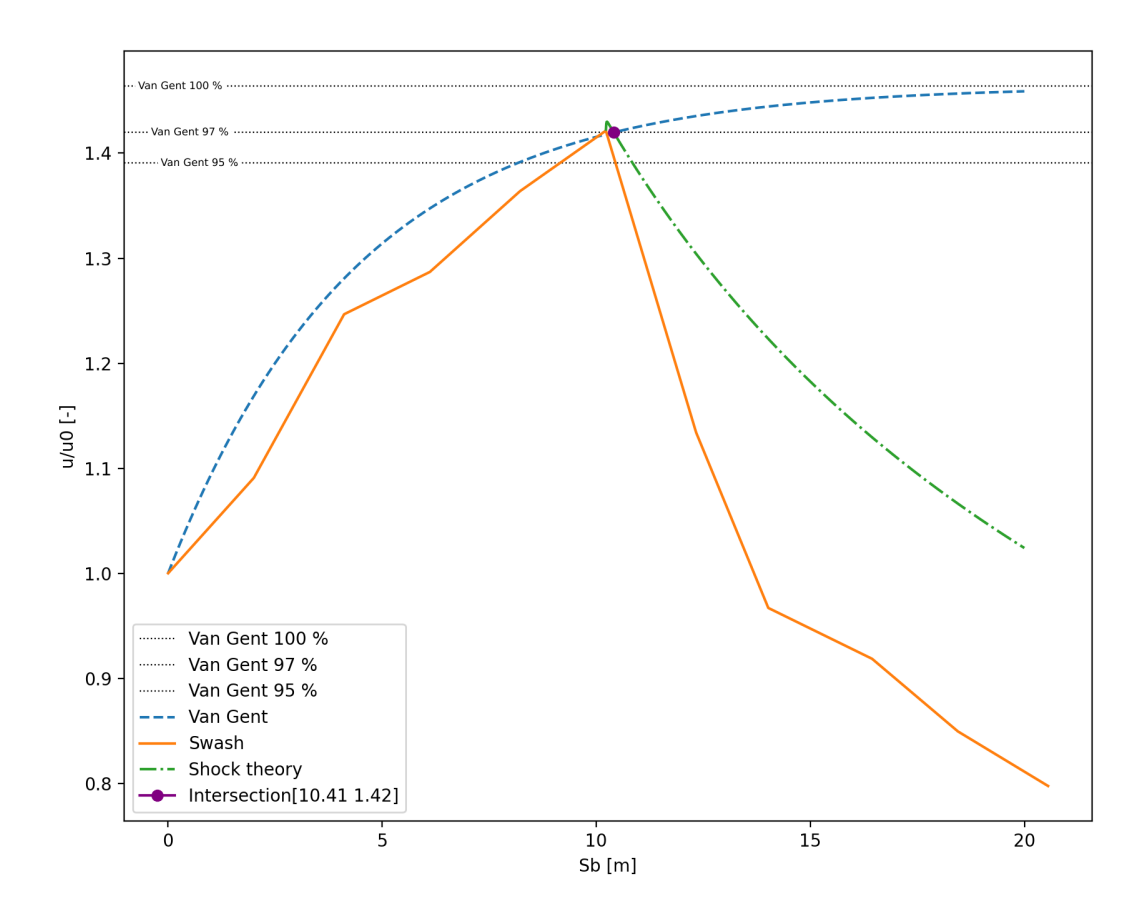


Figure 5.8: Largest wave of the entire simulation, largest is in terms of depth at the end of the crest. The y-axis displays the velocity on the lee side [u] normalized by the starting velocity[ $u_0$ ] at the end of the crest. The x-axis displays the position on the lee side of the dike.

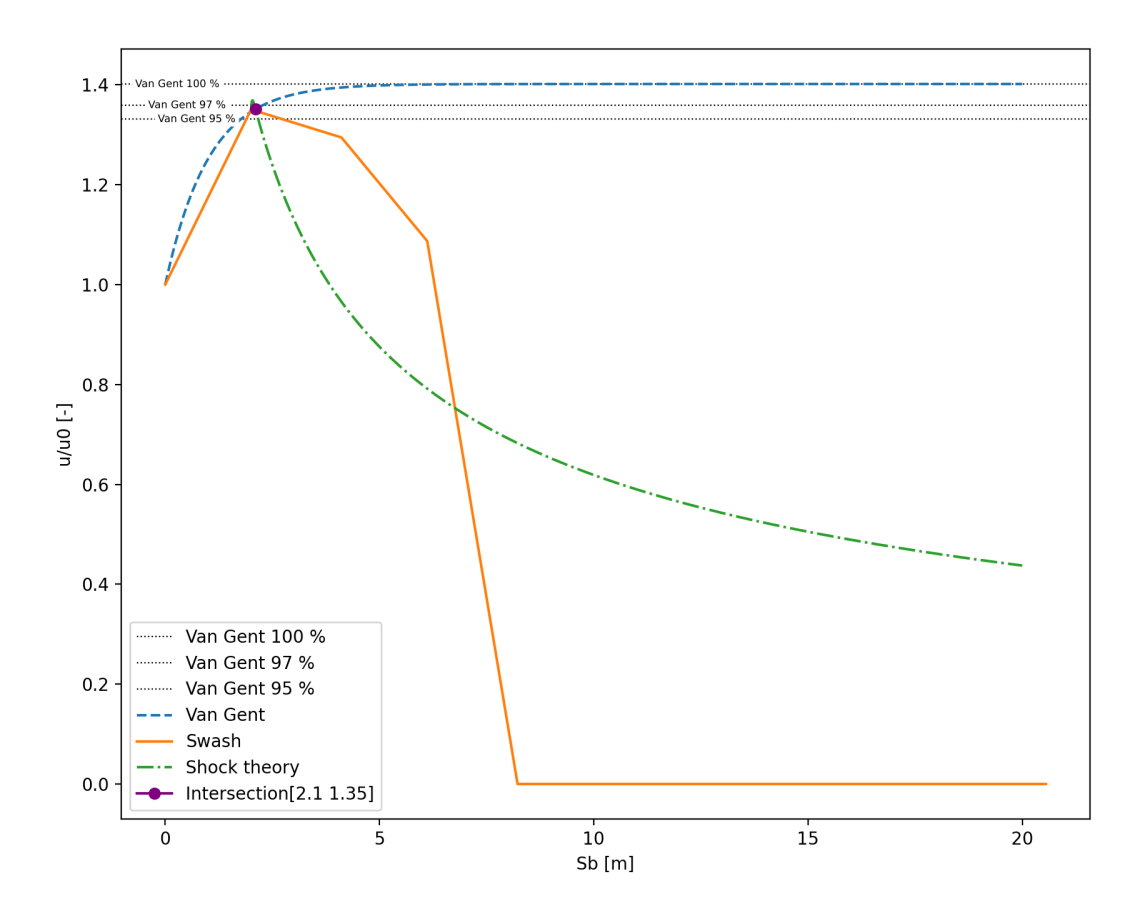


Figure 5.9: Smallest wave of the entire simulation. Smallest is in terms of depth at the end of the crest. The y-axis displays the velocity on the lee side [u] normalized by the starting velocity[ $u_0$ ] at the end of the crest. The x-axis displays the position on the lee side of the dike.

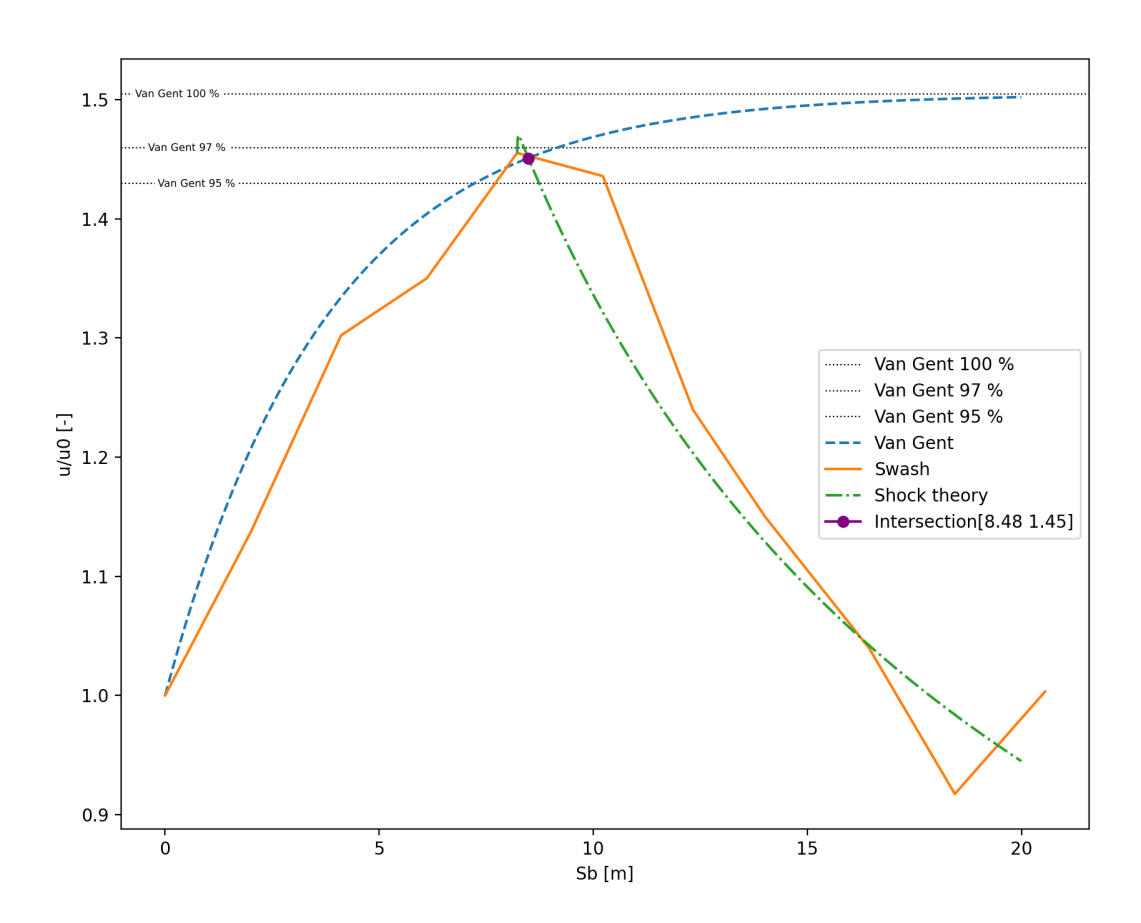


Figure 5.10: Random individual overtopping wave in simulation.

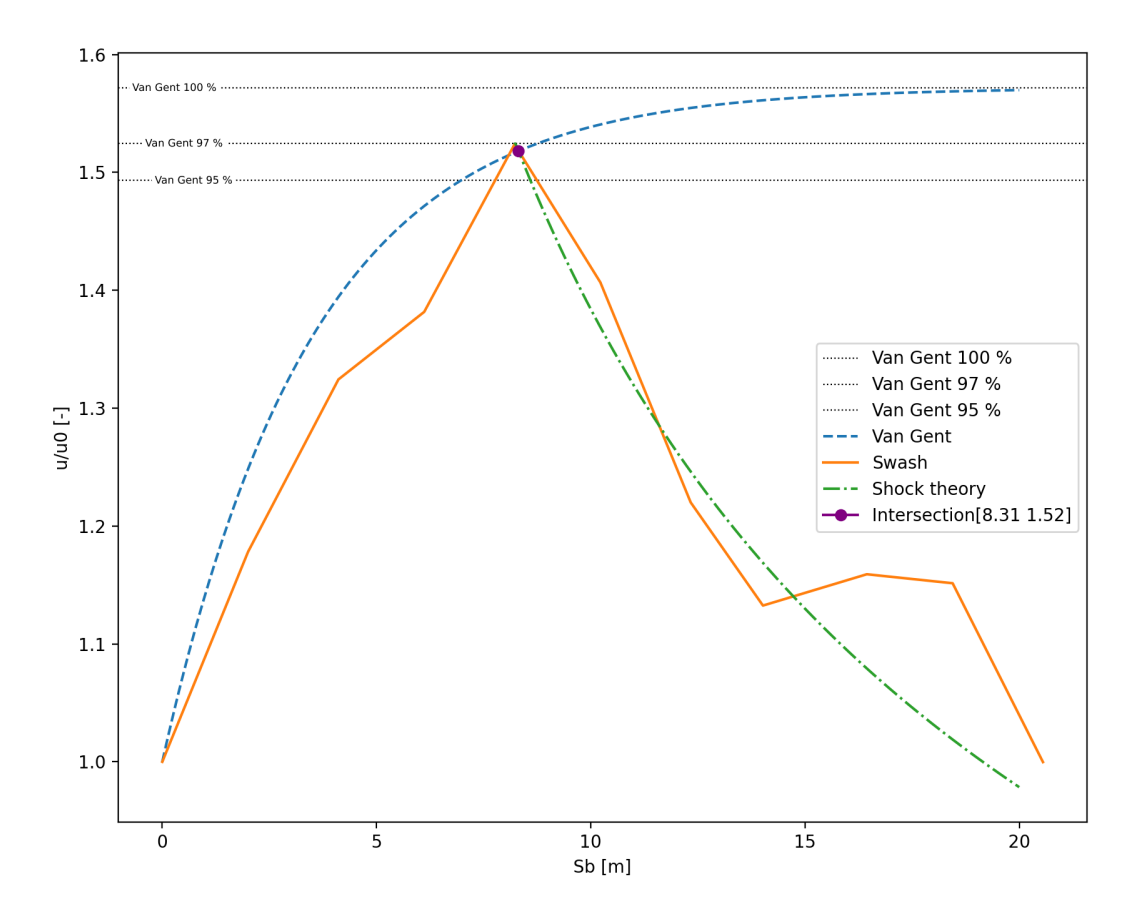


Figure 5.11: Random individual overtopping wave in simulation. The y-axis displays the velocity on the lee side [u] normalized by the starting  $velocity[u_0]$  at the end of the crest. The x-axis displays the position on the lee side of the dike.

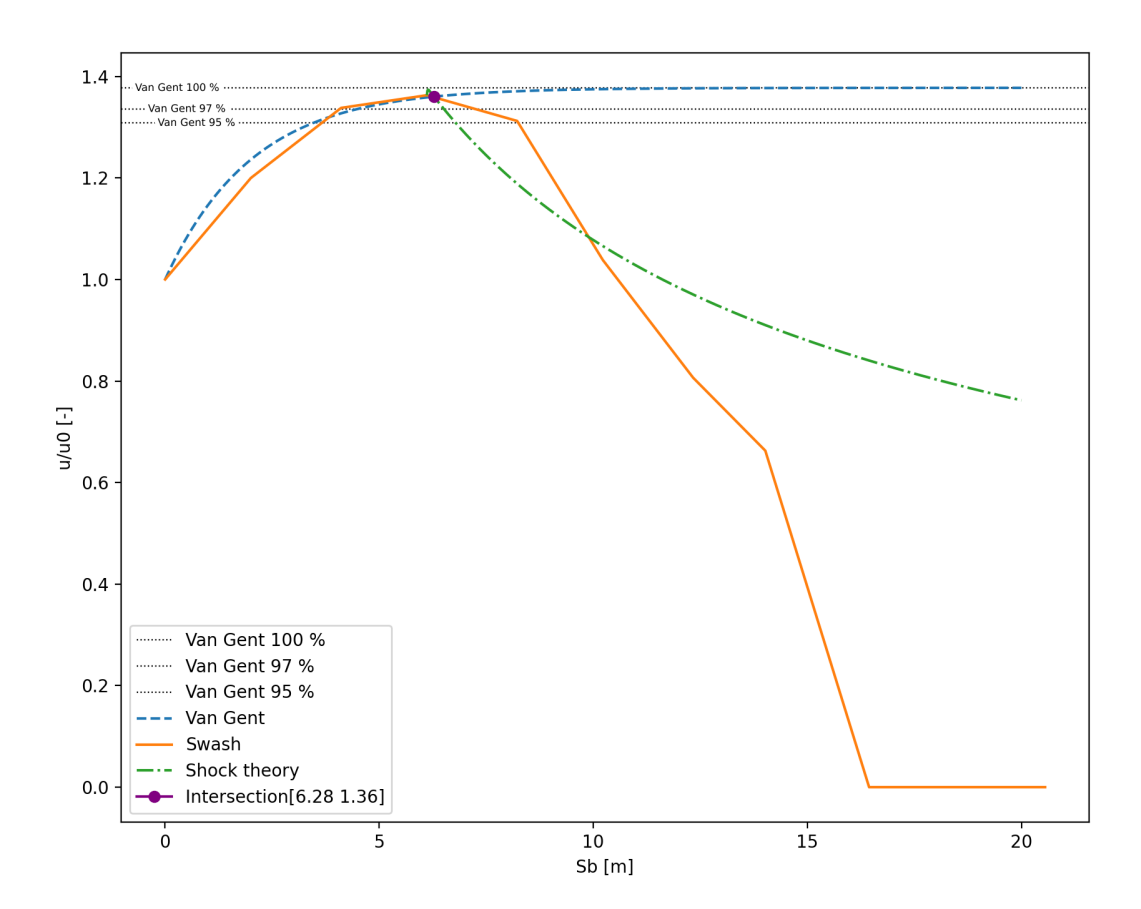


Figure 5.12: Random individual overtopping wave in simulation. The y-axis displays the velocity on the lee side [u] normalized by the starting  $velocity[u_0]$  at the end of the crest. The x-axis displays the position on the lee side of the dike.

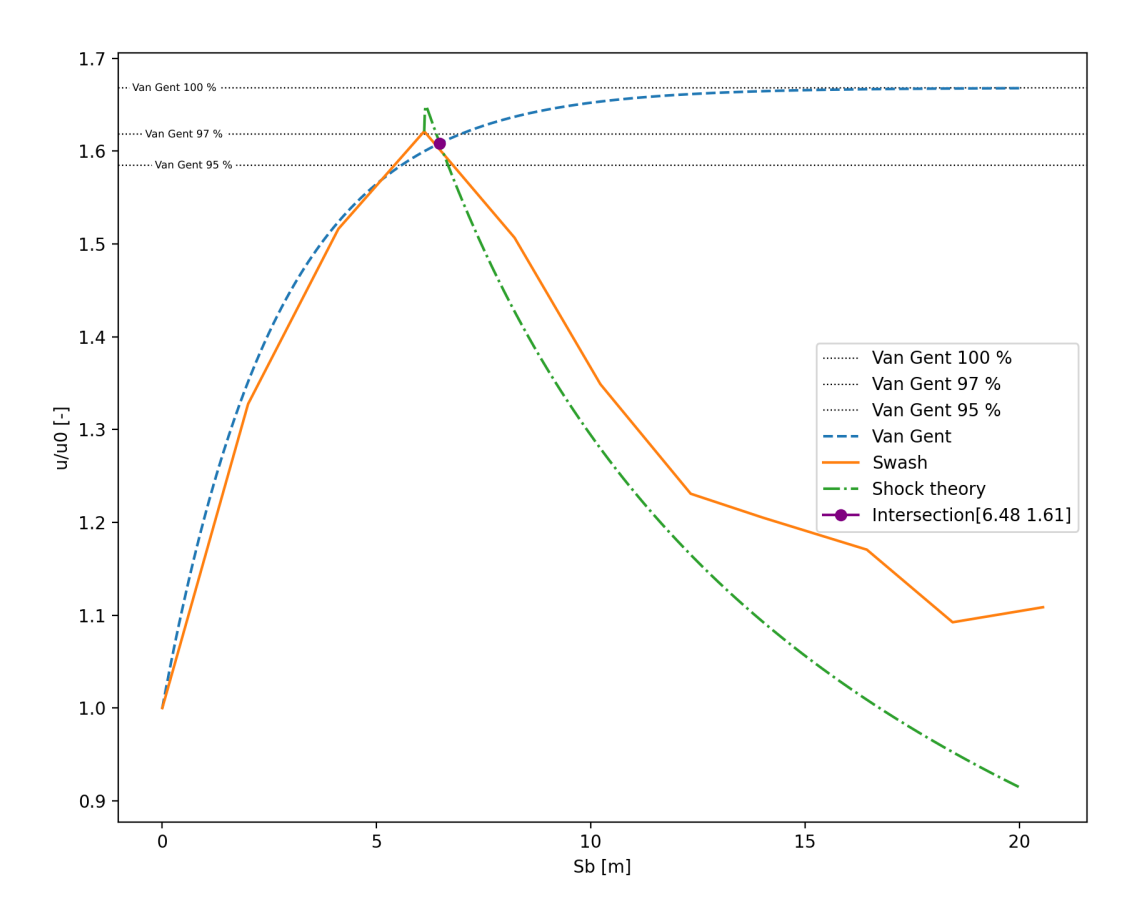


Figure 5.13: Random individual overtopping wave in simulation. The y-axis displays the velocity on the lee side [u] normalized by the starting  $velocity[u_0]$  at the end of the crest. The x-axis displays the position on the lee side of the dike.

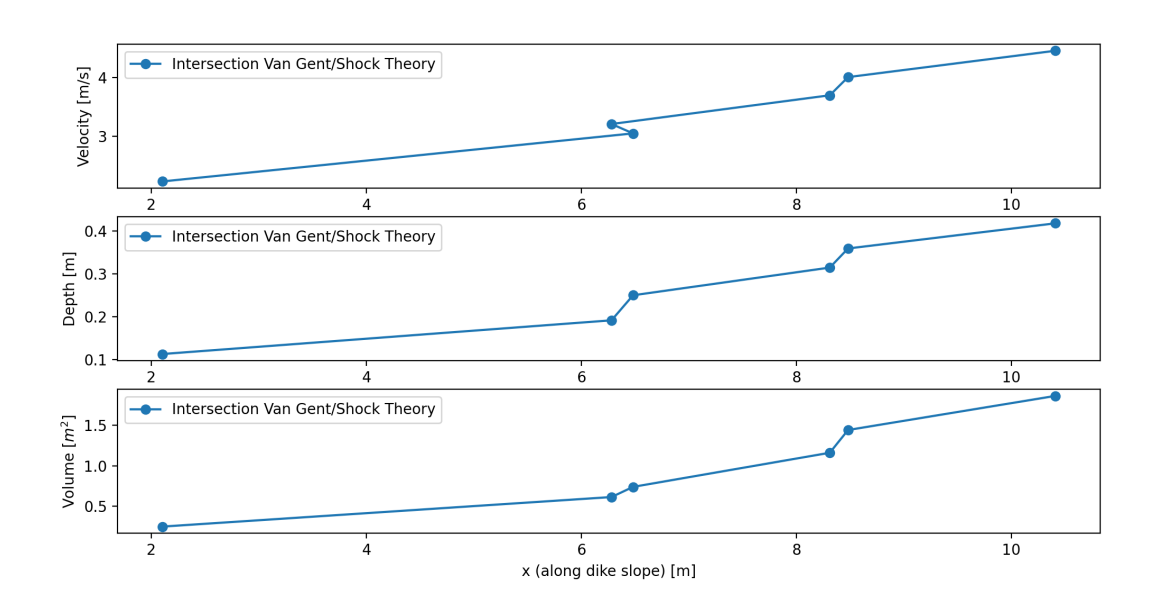


Figure 5.14: Intersection lines, the vertical axis displays the initial depth, velocity or volume of an individual wave at the start of the crest and the horizontal axis displays the position of the tipping point on the lee side of the dike[x] (here x is the same as  $S_B$ ).

### 5.4. Effect different outer slope

To examine whether the flow behaviour described in the previous section was case specific, the WGD simulation is repeated for a variety of outer slope angles. The WGD simulation is repeated for an outer slope of 1:5, 1:6, and 1:8. The wave boundary condition as well as the remaining model settings are kept the same. Expected is that a different outer slope will result in a different q [l/s/m] and Vmax (volume overtopping wave  $[m^3]$ ), which most likely will result in different flow velocities over the crest and lee side of the dike.

In figure 5.15 the results for the cumulative overload method are presented for slopes 1:6 and 1:8 with respect to a 1:7 slope. The x axis represents the measurement points on the crest and lee side of the dike, see figure 4.8 for reference. Without going into detail it is clear that with similar conditions a steeper slope results in a higher cumulative overload value, which indirectly means higher flow velocities on both the crest as well as the lee side.

Figure 5.16 shows the results of the  $u_{2\%}/u_0$  flow velocity on the lee side of the dike for the different outer slope simulations. The y-axis represents  $u_{2\%}/u_0$  and the x axis represents sb, which is the distance along the lee side of the dike. It seems that regardless of the initial velocity at the start of the lee side that the flow velocity initially increases after which it at some point decreases again.

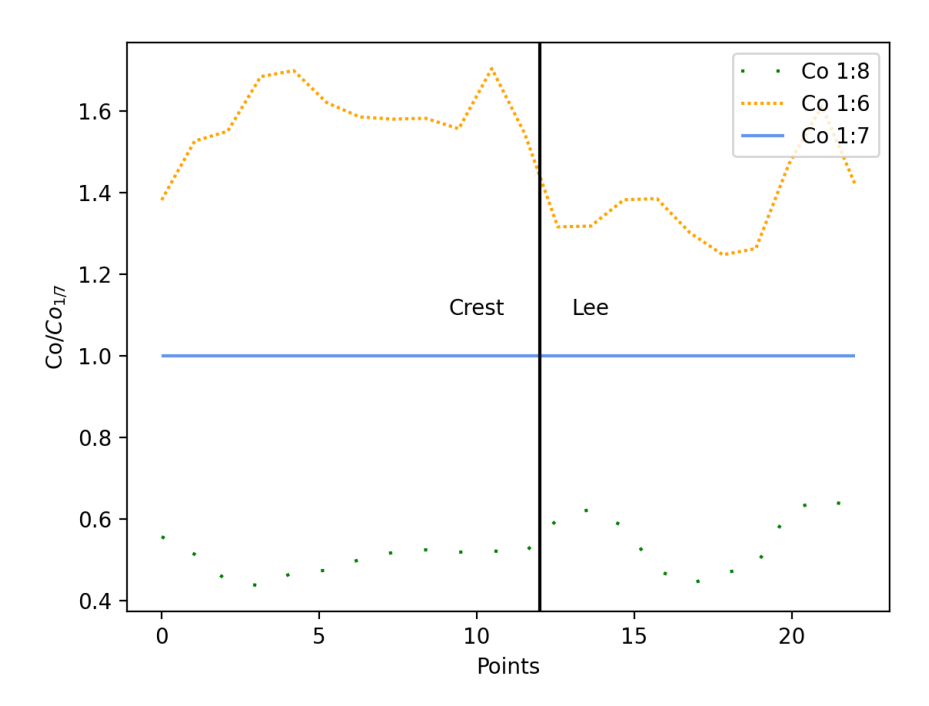


Figure 5.15: co slopes

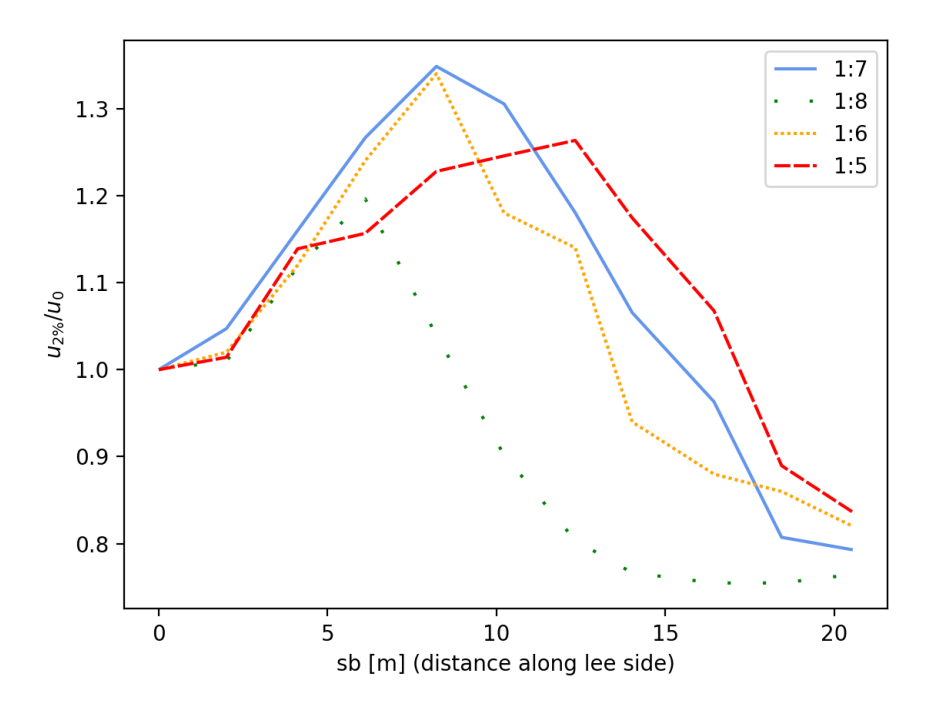


Figure 5.16: lee slopes



## Discussion

#### Wave data

The dike is assessed using wave data extrapolated from the Waddensea. The wave data is input for the seaside boundary. The given wave height/wave period combination at the toe of the dike is very unlikely to exist physically and will therefore probably never occur in real life. This resulted in the formulation of three alternative wave conditions that could function as a boundary. All options are modelled and assessed but only the wave condition that is considered to be the most likely to occur is elaborated on in this report. Because of the sinuous shape of the estuary, the waves being locally generated is assumed to be the most likely to occur. An empirical wind based wave generation derivation is applied to determine the wave conditions that would function as boundary condition. The empirical wind based wave generation derivation uses the water depth as input value. The Dollard is a highly divers coastal system with a large variety of channels and floodplains, resulting in a highly varying bathymetry. The depth parameter for the wind based wave generation derivation is determined in a conservative manner. Still, the varying bathymetry make it a rough estimation of the wave climate.

The used wave conditions are elaborated on extensively. However, the necessary assumptions combined with the complicated natural system allow for uncertainties about the correctness of the wave climate. A dike cannot be optimally designed nor properly assessed if the waves that approach the dike are uncertain. The wave characteristics being uncertain is a knowledge gap that can be resolved by measuring waves in the Dollard. Adding wave measuring devices in the Dollard could also give decisive answer on whether the waves are generated inside or outside the Dollard. As this project is only a 1 km demonstration project, it is recommended to get more insight in the wave climate in the Dollard before the remaining dike surrounding the Dollard is reinforced.

#### **SWASH**

According to literature SWASH can be used for assessing overtopping flows, however, not for such gentle dike slopes up to now. The included SWASH validation to check whether SWASH can be used for assessing overtopping flows on a dike with a gentle outer slope showed reasonable results. Considering overtopping waves, SWASH showed good agreement with the peak flow velocities but overestimated the trailing velocities. The trailing velocities could potentially influence the development of the flows further downstream, therefore SWASH performing less accurate is unfortunate. The SWASH validation was based on one single physical model test, but as SWASH performed only reasonable it is recommended to perform a second validation with more physical model test data. E.g. to examine whether the lower accuracy considering the trailing velocities has a significant impact.

#### Flow on crest

According to literature the flow velocity pattern on the crest is a continuous decrease from the beginning of the crest towards the end of the crest. However, the SWASH model results do not show such a flow velocity pattern. The flow velocity SWASH measurements show an significant initial decrease after which the flow velocity stays roughly the same while the overtopping wave travels towards the end of the crest. Such behaviour indicates that the crest should be wide enough to enable this first flow 52 6. Discussion

velocity decrease but widening the crest even more is not an efficient measure in reducing the flow velocity. Moreover, the current equations for the flow velocity on the crest seem to highly underestimate the flow velocity at the end of the crest. The flow velocity at the end of the crest was around 75%-80% of its initial velocity for each individual simulation, which is higher than the equations predicted. An extended analysis of this behaviour is perhaps an opportunity for future research. An extended analysis is needed to find the optimal crest width in terms of flow velocity decrease, safety and costs.



## Conclusion & Recommendations

The flow depth and flow velocity that would occur for design conditions on the crest and lee side of the WGD is analytically calculated using flow equations by Schüttrumpf, Van Gent and Bosman. These preliminary calculations resulted in very low flow velocities on the crest and lee side. Flow velocities that neither cause failure nor erosion of the dike due to overtopping. Meaning, even with 10 l/s/m of overtopping this results in no erosion of the lee side. Consequently, the 10 l/s/m overtopping criterion would be too strict.

The WGD is designed with boundary conditions provided by HYDRA-NL. A closer look to these boundary conditions, which are wave conditions, indicated that these wave conditions most probably cannot exist physically. This lead to the formulation of a new hydraulic boundary condition. Assuming the waves are generated locally, the new hydraulic boundary condition could reasonably be expected using an empirical wind based wave generation formula. The simulation with this new hydraulic boundary condition resulted in no overtopping. No overtopping logically results in no erosion of the lee side. The overtopping failure criterion is normative for the crest height. If the assumed wave boundary condition appears correct, the results would indicate that there is a reasonable possibility that the dike could be lowered and still guarantee safety.

According to the cumulative overload method 57 l/s/m of overtopping resulted in no initiation of damage. This would indicate that the current correlation between overtopping [l/s/m] and failure of the lee side is oversimplified and an average overtopping of 10 l/s/m will most likely not instantly lead to failure.

As opposed to literature, the flow velocity on the crest showed a much less severe flow velocity decrease over the crest. The observations show a significant initial decrease after which the flow velocity stays roughly the same while the overtopping wave travels along the crest. Such behaviour indicates that the crest should be wide enough to enable this first flow velocity decrease but widening the crest even more is not an efficient measure in reducing the flow velocity. Moreover, the current equations for the flow velocity on the crest highly underestimate the flow velocity at the end of the crest. The flow velocity at the end of the crest was around 75%-80% of its initial velocity for each individual simulation, which is higher than the flow equations predicted.

According to literature the flow velocity on the lee side of a dike initially increases and then eventually stabilizes. However, the SWASH simulation results show after the initial increase also a decrease in flow velocity. The current relations for the flow velocity on the lee side only include the first initial increase but do not include the observed decrease in flow velocity. The kinematic Shock theory equation, could be fitted to the decrease in velocity. The location of the tipping point (change from flow velocity increase to decrease) can be approximated by the location where the flow velocity reaches 97% of its final velocity predicted by Van Gent.

Literature only expects a flow velocity increase on the lee side one would expect the lower part of the lee side to be the most vulnerable to erosion. However, the observed flow velocity decrease shows

that the lowest part of the lee side is perhaps not the location most vulnerable to erosion. A coupled analytical solution for the flow velocity could indicate the locations most vulnerable to erosion, which then could be acted upon.

#### 7.1. Recommendations

Recommendations and opportunities for extended research that follow from the discussion and conclusion are listed below.

#### **Wave climate Dollard**

Any sea dike design is mainly determined by the wave climate. For designing a new dike or assessing an existing dike it is therefore necessary to know the wave climate. The wave climate being uncertain is undesirable. The hydraulic boundary conditions indicate that there is a possibility that the dike could be lowered and still guarantee safety. These hydraulic boundary conditions are however still an assumption, and although reasonable, it is recommended to get more insight in the wave climate of the Dollard to establish a final conclusion. Given the fact that this project is a 1 km demonstration project, it is highly recommended to get more insight into the wave climate in the Dollard (e.g. by adding wave measurement devices) before the remaining dike surrounding the Dollard is reinforced.

#### **SWASH**

SWASH is validated to examine whether SWASH can also be used to assess overtopping flows on a dike with a gentle outer slope. This validation was based on one physical model tests, but as SWASH only performed reasonable it is recommended to perform a second validation with more physical model data.

#### Overtopping criterion

The cumulative overload method indicates that the current overtopping criterion might not be sufficient to optimize dike design. As overtopping criteria are vital in dike design it is key to have a clear understanding of when overtopping causes damage. As a results it is recommended to get more insight in overtopping and resulting damage of the inner slope.

#### **Crest width**

The results indicate that the crest only reduces the flow velocity to a certain extend and suggest that the simply widening the crest width is not an efficient measure to reduce the flow velocity even more. Literature highly underestimated the flow velocity on the crest and consequently also on the lee side. As literature expects the crest to reduce the flow velocity more than the computational model results suggest it is recommended to examine the effect of the crest on reducing the flow velocity.

#### Flow velocity lee side

The initial increase in flow velocity on the lee side is represented by the equation by Van Gent. It seems that the flow velocity decrease can be represented by the kinematic shock theory equation. This suggest that a combination of both formulas represent the flow velocity on the lee side of a dike. It is important to know when to use which formula. The results indicate that the location where the flow velocity after its initial increase starts to decrease again is located at 97% of its final velocity predicted by Van Gent. It is recommended that other configurations are considered to examine if the location for the initiation of flow velocity decrease is constant at 97% of its final velocity predicted by Van Gent.

## Bibliography

- Ahn viewer. (2021). https://www.ahn.nl/ahn-viewer
- Andersen, T., & Burcharth, H. (2004). Clash: D24 report on additional tests: Part a: Effect of obliqueness, short-crested waves and directional spreading.
- Bijlard, R. (2015). Strength of the grass sod on dikes during wave overtopping.
- Bosman, G. (2007). Velocity and flow depth variations during wave overtopping.
- Bosman, G., Van Der Meer, J., Hoffmans, G., Schüttrumpf, H., & Verhagen, H. J. (2009). Individual overtopping events at dikes. in coastal engineering 2008: (in 5 volumes) (pp. 2944-2956).
- Chow, V. (1959). Open-channel hydraulics. mcgraw hiu.
- De Roo, S., Suzuki, T., Kolokythos, G., Zhao, G., & Verwaest, T. (2015). Numerical modelling of 2d wave transformation processes from nearshore to a shallow foreshore: Comparison between the mike21, swash and xbeach models. in 36th iahr world congress (pp. 1-6).
- Dean, R. G., Rosati, J. D., Walton, T. L., & Edge, B. L. (2010). Erosional equivalences of levees: Steady and intermittent wave overtopping. ocean engineering, 37(1), 104-113.
- Dijk, S. (2021). Project brede groene dijk. https://eemsdollard2050.nl/project/brede-groene-dijk/
- Duits, M. (2020). Hydra-nl gebruikershandleiding. Rijkswaterstaat Water, Verkeer en Leefomgeving.
- Eurotop [Manual on wave overtopping of sea defences and related structures]. (2018).
- Gruwez, V., Altomare, C., Suzuki, T., Streicher, M., Cappietti, L., Kortenhaus, A., & Troch, P. (2020). An inter-model comparison for wave interactions with sea dikes on shallow foreshores. journal of marine science and engineering, 8(12), 985.
- Het verhaal van de eems-dollard. (2021). https://eemsdollard2050.nl/over-het-programma/ons-verhaal/
- Hoffmans, G., Akkerman, G. J., Verheij, H., van Hoven, A., & Van Der Meer, J. (2008). The erodibility of grassed inner dike slopes against wave overtopping. in coastal engineering 2008: (in 5 volumes) (pp. 3224-3236).
- Holthuijsen, L. H. (2007). Waves in oceanic and coastal waters. Cambridge university press.
- Hughes, S., & Nadal, N. (2009). Laboratory study of combined wave overtopping and storm surge overflow of a levee. coastal engineering, volume 56, issue 3, march 2009, pages 244-259.
- Jonkman, S. N., Hillen, M. M., Nicholls, R. J., Kanning, W., & van Ledden, M. (2013). Costs of adapting coastal defences to sea-level rise—new estimates and their implications. journal of coastal research.
- Kamphuis, J. W. (1997). Experiments on design wave height in shallow water. in coastal engineering 1996 (pp. 221-232).
- Kennedy, A., Chen, Q., Kirby, J., & Dalrymple, R. (2000). Boussinesq modeling of wave transformation, breaking, and runup. i: 1d. journal of waterway, port, coastal, and ocean engineering 1260 (1), 39–47..
- Kremer, R. H. J., Van der Meer, M. T., Niemeijer, J., Koehorst, B. A. N., & Calle, E. O. F. (2001). *Technisch rapport waterkerende grondconstructies; geotechnische aspecten van dijken, dammen en boezemkaden.*
- Lighthill, M. J., & Whitham, G. B. (1955). On kinematic waves i. flood movement in long rivers. proceedings of the royal society of london. series a. mathematical and physical sciences, 229(1178), 281-316.
- Rijkswaterstaat. (2021a). Dijken. https://www.rijkswaterstaat.nl/water/waterbeheer/bescherming-tegen-het-water/waterkeringen/dijken
- Rijkswaterstaat. (2021b). Ruimte voor de rivieren. https://www.rijkswaterstaat.nl/water/waterbeheer/bescherming-tegen-het-water/maatregelen-om-overstromingen-te-voorkomen/ruimte-voorde-rivieren
- Rijkswaterstaat. (2021c). Waterkeringen. https://www.rijkswaterstaat.nl/water/waterbeheer/beschermingtegen-het-water/waterkeringen
- Schematiseringshandleiding grasbekleding. (2021). Rijkswaterstaat Water Verkeer en Leefomgeving.

56 Bibliography

Schiereck, G., & Verhagen, H. (2012). *Introduction to bed, bank and shore protection 2nd edition.* Delft Academic Press / VSSD.

- Schüttrumpf, H. (2001). Wellenüberlaufströmung an seedeichen: Experimentelle und theoretische untersuchungen (doctoral dissertation).
- Schüttrumpf, H., & Oumeraci, H. (2005). Layer thicknesses and velocities of wave overtopping flow at seadikes. coastal engineering, 52(6), 473-495.
- Schüttrumpf, H., Oumeraci, H., Möller, J., & Kudella, M. (2001). Loading of the inner slope of seadikes by wave overtopping. leichtweiss institut für wasserbau technical university braunschweig.
- Singh, V. P. (2017). Kinematic wave theory of overland flow. water resources management, 31(10), 3147-3160. iso 690.
- Smit, P., Zijlema, M., & Stelling, G. (2013). Depth-induced wave breaking in a non-hydrostatic, near-shore wave model. coastal engineering, 76, 1-16.
- Smith, G., Seijffert, J., & Van der Meer, J. (1994). Erosion and overtopping of a grass dike large scale model tests. in coastal engineering.
- Steendam, G. J., Hoffmans, G., Bakker, J., van der Meer, J., Frissel, J. Y., Paulissen, M. P. C. P., & Verheij, H. J. (2012). Sbw wave overtopping and grass cover strength, model developement.
- Steendam, G., van Hoven, A., & Van der Meer, J. (2015). Validation of cumulative overload method based on tests by the new wave run-up simulator.
- Suzuki, T., Altomare, C., Veale, W., Verwaest, T., Trouw, K., Troch, P., & Zijlema, M. (2017). Efficient and robust wave overtopping estimation for impermeable coastal structures in shallow foreshores using swash. coastal engineering, 122, 108-123.
- SWECO. (2021a). Brede groene dijk: Een unieke dijk van klei, goed voor mens en natuur. https://www.sweco.nl/portfolio/duurzame-brede-groene-dijk/
- SWECO. (2021b). Do ontwerp voor brede groene dijk fase 3a op basis inzichten eerste deltagootproef. TU-Delft. (2021). Swash manual. https://swash.sourceforge.io/online\_doc/swashuse/swashuse.html
- UVW. (2021). Kerngegevens waterschappen. https://www.uvw.nl/wp-content/files/Factsheet%5C% 20Kerngegevens%20waterschappen%202011.pdf
- Van Bergeijk, V., Warmink, J., Van Gent, M., & Hulscher, S. (2019). An analytical model of wave overtopping flow velocities on dike crests and landward slopes.
- Van den Bos, W. (2006). Erosiebestendigheid van grasbekleding tijdens golfoverslag.
- Van der Meer, J. (2002). Technical report wave run-up and wave overtopping at dikes. taw report (incorporated in the eurotop manual). engineering.
- Van der Meer, J., Hoven, A. V., Paulissen, M., Steendam, G. J., Verheij, H., Hoffmans, G., & Kruse, G. (2015). *Handreiking dijkbekledingen-deel 5: Grasbekledingen*.
- Van Der Meer, J. W., Hardeman, B., Steendam, G. J., Schüttrumpf, H., & Verheij, H. (2010). Flow depths and velocities at crest and landward slope of a dike, in theory and with the wave overtopping simulator. coastal engineering proceedings, 1(32), 10.
- Van der Meer, J., Bernardini, P., Snijders, W., & Regeling, E. (2006). The wave overtopping simulator. Van Gent, M. (2001). Low-exceedance wave overtopping events: Estimates of wave overtopping parameters at the crest and landward side of dikes. dc1-322-1.
- Van Gent, M. (2002). Low-exceedance wave overtopping events: Measurements of velocities and the thickness of water-layers on the crest and inner slope of dikes.
- Van Gent, M., & Schüttrumpf, H. (2004). Wave overtoppping at seadikes.
- van Bergeijk, V. M., Verdonk, V. A., Warmink, J. J., & Hulscher, S. J. (2021). The cross-dike failure probability by wave overtopping over grass-covered and damaged dikes. water, 13(5), 690. iso 690.
- Waterschap-Hunze-en-Aa's. (2021). Over ons. https://www.hunzeenaas.nl
- Ysebaert, T., van der Wal, J. T., Tangelder, M., de Groot, A. V., & Baptist, M. J. (2016). Ecotopenkaart voor het eems-dollard estuarium (no. c059/15). imares.



# Hand calculation flow crest and lee side WGD

This appendix contains an elaboration of the flow calculations for the crest and lee side of the WGD using flow equations from Schüttrumpf and Van Gent discussed in chapter 2.

**Parameter** Value  $\overline{H_{m0}}$  [m] 2.33  $T_{m-1,0}$  [s] 4.01 Outer slope [-] 1/7 Inner slope [-] 1/3 0.95  $\gamma_B$  [-] 0.91  $\gamma_{\beta}$  [-]  $\gamma_f$  [-] 1 Freeboard [m] 1.01

Table A.1: Calculation values to start calculation

The first step is to calculate the peak period (see equation A.1, Kremer et al., 2001).

$$T_{peak} = 1.1 \cdot T_{m-1,0} = 1.1 \cdot 4.01 = 4.41s$$
 (A.1)

The next step is to calculate the deep water wave length(see equation A.2). In this equation the wave period [T] and wave length [L] are not yet specified. The next step is to calculate the Iribarren parameter. The Iribarren parameter for irregular wave requires the deep water wave length  $[L_{op}]$  using the peak period  $[T_p]$  (Schiereck and Verhagen, 2012). It follows that the subscript T and L in equation A.2 are respectively  $T_p$  and  $L_{op}$ .

$$L = \frac{g \cdot T^2}{2\pi} \xrightarrow{Irregular-waves} L_{op} = \frac{g \cdot T_p^2}{2\pi} = \frac{9.81 \cdot 4.41^2}{2\pi} = 30.4m \tag{A.2}$$

The Iribarren parameter is calculated using equation A.3.

$$\xi_{m-1,0} = \frac{\tan \alpha}{\sqrt{\frac{H_{m0}}{L_{op}}}} = \frac{\tan^{-1}(1/7)}{\sqrt{\frac{2.33}{30.4}}} = 0.51$$
 (A.3)

The next step is to calculate the run up. The run up is calculated using equation 2.2 (equation A.4 in the appendix). The Eurotop manual (*Eurotop*, 2018) presents an equation for the run up (equation 2.2) and a maximum run up (equation 2.3). The equation for the run up appears normative and the equation for the maximum run up is therefore not mentioned here.

$$R_{u2\%} = H_{m0} \cdot 1.75 \cdot \gamma_b \cdot \gamma_f \cdot \gamma_\beta \cdot \xi_{m-1,0} = 2.33 \cdot 1.75 \cdot 0.95 \cdot 0.91 \cdot 1 \cdot 0.51 = 1.81m \tag{A.4}$$

#### A.1. Flow seaward

This section contains an elaboration of the flow calculations(see equations 2.9 and 2.10) on the seaward slope of the dike. For this calculation table 2.2 and table 2.3 are needed. The values derived from these equations are at the end of the seaward slope and at the start of the crest.

#### Schüttrumpf

$$u_{A,2\%} = \sqrt{gH_S} \cdot c_{A,u}^* \cdot \sqrt{\frac{R_{u,2\%} - z_A}{H_S}} = \sqrt{9.81 \cdot 2.33} \cdot 1.37 \cdot \sqrt{\frac{1.81 - 1.01}{2.33}} = 3.85 m/s \tag{A.5}$$

$$h_{A,2\%} = H_S \cdot c_{A,h}^* \cdot (\frac{R_{u,2\%} - z_A}{H_S}) = 2.33 \cdot 0.33 \cdot \frac{1.81 - 1.01}{2.33} = 0.27m$$
 (A.6)

Van Gent

$$u_{A,2\%} = \sqrt{gH_S} \cdot c_{A,u}^* \cdot \sqrt{\frac{R_{u,2\%} - z_A}{H_S}} = \sqrt{9.81 \cdot 2.33} \cdot 1.3 \cdot \sqrt{\frac{1.81 - 1.01}{2.33}} = 3.65 m/s \tag{A.7}$$

$$h_{A,2\%} = H_S \cdot c_{A,h}^* \cdot (\frac{R_{u,2\%} - z_A}{H_S}) = 2.33 \cdot 0.15 \cdot \frac{1.81 - 1.01}{2.33} = 0.12m$$
 (A.8)

**Bosman** 

$$u_{A,2\%} = \sqrt{gH_S} \cdot c_{A,u}^* \cdot \sqrt{\frac{R_{u,2\%} - z_A}{H_S}} = \sqrt{9.81 \cdot 2.33} \cdot 2.12 \cdot \sqrt{\frac{1.81 - 1.01}{2.33}} = 5.96 m/s \tag{A.9}$$

$$h_{A,2\%} = H_S \cdot c_{A,h}^* \cdot (\frac{R_{u,2\%} - z_A}{H_S}) = 2.33 \cdot 0.45 \cdot \frac{1.81 - 1.01}{2.33} = 0.36m$$
 (A.10)

#### A.2. Flow crest

This section contains an elaboration of the flow calculations on the crest. The calculations uses the following equations 2.11, 2.12, 2.14 and 2.13. Furthermore tables 2.4 and 2.5 are needed. The crest has a width of 11 m (B = 11 m). The flow velocity and flow height is presented at the end of the crest, meaning  $x_c$  = 11 m. A value of 0.01 is used for friction parameter f (van Bergeijk et al., 2021).

#### Schüttrumpf

$$u_{c,2\%} = u_{A,2\%}(R_C) \cdot exp(-c_{c,u}^* \cdot \frac{x_c \cdot f}{h_{c,2\%}}) = 3.85 \cdot exp(-0.5 \cdot \frac{11 \cdot 0.01}{0.12}) = 2.32m/s \tag{A.11}$$

$$h_{c,2\%} = h_{A,2\%}(R_C) \cdot exp(-c_{c,h}^* \cdot \frac{x_c}{B}) = 0.27 \cdot exp(-0.89 \cdot \frac{11}{11}) = 0.12m$$
 (A.12)

Van Gent

$$u_{c,2\%} = u_{A,2\%}(R_C) \cdot exp(-c_{c,u}^* \cdot \frac{x_c \cdot f}{h_{c,2\%}}) = 3.65 \cdot exp(-0.5 \cdot \frac{11 \cdot 0.01}{0.08}) = 1.85 m/s$$
 (A.13)

$$h_{c,2\%} = h_{A,2\%}(R_C) \cdot exp(-c_{c,h}^* \cdot \frac{x_c}{B}) = 0.27 \cdot exp(-0.4 \cdot \frac{11}{11}) = 0.08m$$
 (A.14)

**Bosman** 

$$u_{2\%}(x_c) = u_{2\%}(x_c = 0) \cdot exp(-c_{u,2\%} \cdot \frac{x_c}{\gamma_c \cdot h_{2\%}(x_c)}) = 5.96 \cdot exp(-0.042 \cdot \frac{11}{1 \cdot 0.002} = 0m/s \quad (A.15)$$

$$h_{2\%}(x_c) = h_{2\%}(x_c = 0) \cdot c_{trans,h} \cdot \exp(-c_{h,2\%} \cdot \frac{x_c}{\gamma_c \cdot L_0}) = 0.36 \cdot 0.81 \cdot exp(-15 \cdot \frac{11}{1 \cdot 30.4}) = 0.001m \text{ (A.16)}$$

A.3. Flow lee side 59

#### A.3. Flow lee side

This section contains an elaboration of the flow calculations on the lee side. For this calculation the equation derived by Van Gent are used(see equation 2.20). The calculation is done twice, once with input values from the results of the Van Gent crest calculation (equation A.13 and equation A.14 and once with the input values from the results of the Bosman crest calculation (equation A.15 and equation A.16). The parameter  $S_B$  is chosen to be 10 m.

#### Van Gent (Van Gent input values)

$$u_{B,2\%} = \frac{k_2}{k_3} + k_4 \cdot exp(-3 \cdot k_2 \cdot k_3^2 \cdot s_B) = \frac{1.49}{0.32} - 2.79 \cdot exp(-3 \cdot 1.49 \cdot 0.32^2 \cdot 10) = 4.6m/s \quad (A.17)$$

With:

$$k_2 = \sqrt[3]{g \cdot \sin\phi} \sqrt[3]{9.81 \cdot 1/3} = 1.49$$
 (A.18)

$$k_3 = \sqrt[3]{\frac{1}{2} \frac{f}{h_{0,2\%} \cdot u_{0,2\%}}} = \sqrt[3]{\frac{1}{2} \frac{0.01}{0.08 \cdot 1.85}} = 0.32$$
 (A.19)

$$k_4 = u_{0,2\%} - \frac{k_2}{k_3} = 4.7 \cdot 10^{-26} - \frac{1.49}{0.32} = -2.79$$
 (A.20)

#### Van Gent (Bosman input values)

$$u_{B,2\%} = \frac{k_2}{k_3} + k_4 \cdot exp(-3 \cdot k_2 \cdot k_3^2 \cdot s_B) = \frac{1.49}{6.1 \cdot 10^{28}} - 2.45 \cdot 10^{-29} \cdot exp(-3 \cdot 1.49 \cdot (6.1 \cdot 10^{28})^2 \cdot 10) = 0m/s$$
(A.21)

With:

$$k_2 = \sqrt[3]{g \cdot \sin\phi} = \sqrt[3]{9.81 \cdot 1/3} = 1.49$$
 (A.22)

$$k_3 = \sqrt[3]{\frac{1}{2} \frac{f}{h_{0,2\%} \cdot u_{0,2\%}}} = \sqrt[3]{\frac{1}{2} \frac{0.01}{0.002 \cdot 0}} = \infty$$
 (A.23)

$$k_4 = u_{0,2\%} - \frac{k_2}{k_3} = 1.05 \cdot 10^{-86} - \frac{1.49}{6.1 \cdot 10^{28}} = -\infty$$
 (A.24)